UNIVERSITÀ DEGLI STUDI DI PADOVA

Dipartimento di Fisica e Astronomia "Galileo Galilei"

Master Degree in Physics

Master's Degree dissertation

Measurement forecasts of the ultra-high-energy neutrino flavor composition: unlocking new insights into astrophysics and fundamental physics

Thesis supervisor

Prof. Elisa Bernardini

Thesis co-supervisors

Prof. Mauricio Bustamante

Dr. Damiano F. G. Fiorillo

Candidate

Federico Testagrossa

Academic Year 2023/2024

Abstract

The neutrinos of cosmic origin discovered by the IceCube detector, with TeV–PeV energies, unlocked new perspectives on high-energy non-thermal astrophysical sources and high-energy fundamental physics. It is therefore captivating to extend our reach to higher energies, where neutrinos will connect us to the most extreme phenomena of our Universe. In the upcoming decade, a new generation of neutrino telescopes, currently under planning, will target the discovery of ultra-high-energy (UHE) neutrinos, with EeV-scale energies, predicted in the late 1960s. Discovering UHE neutrinos would shed light on the origin and production mechanism of the most energetic cosmic rays, and also allow us to probe neutrino physics at energies otherwise unattainable. A versatile tool to test both aspects is their flavor composition, *i.e.*, the fraction of neutrinos of each flavor in the total flux. However, measuring the flavor content of UHE neutrinos would require individual UHE neutrino telescopes to have flavor-identification capabilities. This is not guaranteed, even though research is ongoing. In this work, we propose and explore a novel idea to measure the UHE neutrino flavor composition that circumvents this potential obstacle. Flavor sensitivity is manufactured from the joint detection by two telescopes, one sensitive to all flavors—the radio array of IceCube-Gen2—and one mostly sensitive to ν_τ —GRAND. Even under conservative choices of neutrino flux and detector size, this flavor sensitivity, predominantly to ν_τ, is sufficient to extract new insight. This work presents the first measurement forecasts of the UHE ν_τ content. Then, these forecasts are used for astrophysics, where they give meaningful constraints on the neutrino production mechanism, and for fundamental physics, improving by many orders of magnitude the constraints on Lorentz-invariance violation.

Ved gamle Borg
i kolde Mose,
stod taus i Sorg
den röde Rose.
Den lumske Orm
vil Rosen nage.
O haarde Storm!
Den maa forsage.

Contents

Chapter 1

Neutrino Physics

1.1 A brief history of neutrinos

Neutrinos are neutral spin-1/2 fermions that interact only via weak interactions in the Standard Model of particle physics. Their history covers a whole century, but even after a long research campaign, which is even more active today, they stand among the most uncanny characters in our theories of the fundamental interactions.

The early tales of neutrinos are strongly tied to the birth and development of nuclear science: since the discovery of radioactivity by Henry Becquerel in 1896, people began to study the radiations spontaneously emitted by certain minerals, finding out that they were of three types, called α, β and γ. β radiation was soon understood to be made of electrons, but its spectrum seemed to be inconsistent with the nuclear models of the time.

Indeed, back then only protons and electrons were known, and these were thought to be the building blocks of the nucleus. To explain β radiation, people believed that sometimes one of the electrons contained in the nucleus was emitted, leading to a two-body decay to a different nucleus–the β-decay. Problems arose when, 20 years after the discovery of β radiation, scientists were able to measure with precision the spectrum of this decay; it was a continuum spectrum and terminated, within the energy resolution, at the energy that one would have expected in a two-body decay, by energy-momentum conservation. Moreover, this model predicted some nuclei, such as ^{14}N, to be fermions, while they were behaving as bosons.

How to reconcile theory with experiments? The correct answer was eventually given by Wolfgang Pauli in 1930. In order not to give up energy conservation and spin-statistics theorem, he proposed the existence of a new particle [1], which he baptized the *neutron*, that had to be neutral and of spin-1/2. Enrico Fermi, given the small mass scale expected for this particle, proposed the name *neutrino*, ν, and what we call neutron was discovered soon after by James Chadwick, in 1932 [2].

When Fermi wrote his successful theory for the β decay of nuclei [3], for which its origin is the three-body decay of the neutrons inside the nucleus, $n \to e^- + p + \bar{\nu}_e$, he also realized that, in order to explain the data, the strength of the fundamental interaction mediating this process should have been orders-of-magnitude weaker than the electromagnetic interaction. β decay and its crossed processes ($p \to n + e^+ + \nu_e$ and $p + e^- \to n + \nu_e$) were the only known sources of neutrinos; thus, the hope to detect and discover this new particle was challenged by its expected weak interactions

with matter. To compensate this problem, an intense source of neutrinos was needed, so experiments were built in the proximity of nuclear reactors.

Finally, the neutrino was discovered by Frederick Reines and Clyde Cowan, in 1956 [4, 5]. Neutrinos, more specifically electron anti-neutrinos, were detected for the first time via the inverse beta decay,

$$\bar{\nu}_e + p \to n + e^+ \ ,$$

at the Savannah River experiment, where two tanks of water enriched with cadmium (Cd) were placed as target for the intense flux of neutrinos coming from the nearby nuclear reactor. The resulting positron would annihilate with atomic electrons, producing two photons in opposite directions, while the neutrons would have been captured by Cd nuclei, leading to an excited state that would decay emitting a γ. Looking for the coincident detection of two γ from pair annihilation, followed by the delayed detection of the γ from Cd decay, Reines and Cowan found a rate of three events per hour, which disappeared when the reactor was shut down. This confirmed the existence of the neutrino, 26 years after Pauli's intuition. Moreover, the cross section measured for the inverse beta decay was compatible with the one predicted by Fermi's theory.

This groundbreaking discovery catalyzed a multitude of new research directions in Physics, which are still active today. Among these, we will retrace the solar neutrino problem and discuss its resolution in the theory of neutrino oscillations, as it will be an important tool for our work.

1.2 The oscillation puzzle

Soon after the discovery of the neutrino, it was realized that a flux of this particle could come not only from nuclear reactors on Earth, but also from extraterrestrial sources. Indeed, stars such as our Sun are fueled by chains of nuclear reactions, in which neutrinos are produced with MeV scale energies. Fig. 1.1 [6] shows the different contribution to the flux of solar neutrinos. The flux of solar neutrinos is orders of magnitude smaller than the one detected at the Savannah River experiment, so new detection techniques were necessary.

The first successful attempt was carried out in the late 1960s, in a radiochemical experiment at the Homestake gold mine in South Dakota. This experiment, led by Raymond Davis and John Bahcall, consisted in a huge tank of perchloroethylene, interacting with solar neutrinos via the inverse beta process

$$\nu_e + {}^{37}\mathrm{Cl} \to {}^{37}\mathrm{Ar}^+ + e^- \ .$$

The ${}^{37}\mathrm{Ar}^+$ atoms produced would not interact with the chlorine, and were stable enough to be counted as byproducts of the interactions of solar neutrinos. The experiment detected for the first time solar neutrinos, but it measured a flux equal to one third of the theoretical expectation [7, 8]. Although such a discrepancy was the first hint towards new physics, its theoretical calculations relied on the Standard Solar Model, which could also be the problem. In order to make any claim, new measurements, complementary to the Homestake results, were necessary, together with more robust calculations.

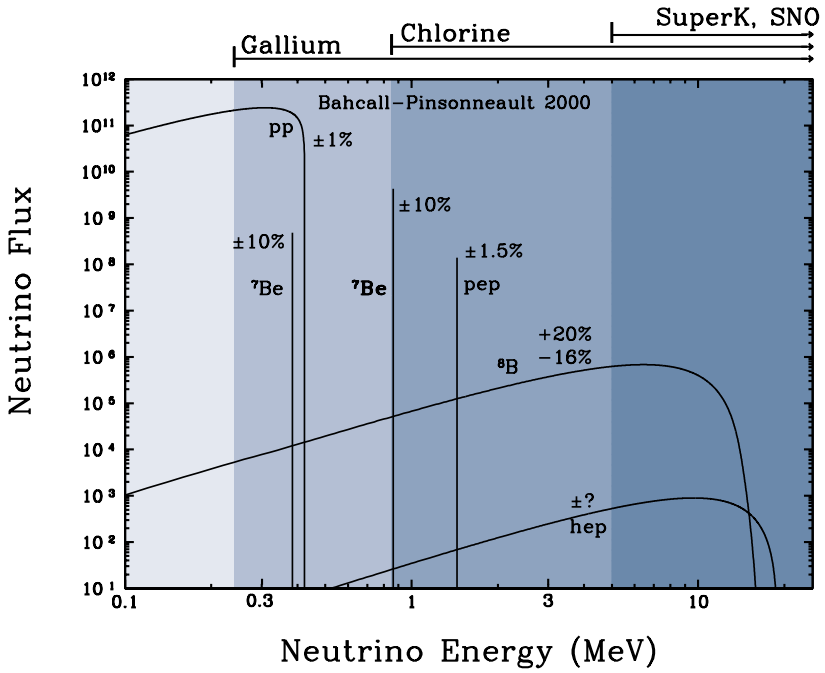

Figure 1.1: **Flux of solar neutrinos.** *The fluxes are in* $\mathrm{cm}^{-1}\ \mathrm{s}^{-1}$ *and stem from different nuclear reactions, with the theoretical uncertainties due to the uncertain fraction of heavier nuclei. Colors represent the threshold for different experimental techniques, discussed in the chapter. Figure taken from Ref. [6].*

To this end, new experiments were built, targeting a different energy window of the spectrum of solar neutrinos. The experiments GALLEX, in Italy, and SAGE, in the Soviet Union, used volumes of liquid gallium to observe the reaction [9]

$$\nu_e + {}^{71}\mathrm{Ga} \rightarrow {}^{71}\mathrm{Ge} + e^- \ .$$

Again, extracting and counting the germanium it was possible to measure the number of neutrino interactions. The threshold for this reaction was lower than the one observed in the Homestake experiment, so these experiments were able to detect lower energy neutrinos. In particular, they were sensitive to the ν_e produced in the proton-proton ($p-p$) chain, which is the most efficient reaction happening in the Sun. A larger flux of solar neutrinos, and more reliable calculations for the well-known p-p chain, were available. Nonetheless, a discrepancy between theory and experience was found again [10, 11].

As the mystery of solar neutrinos, later called the solar neutrino problem, deepened, the properties of this ghostly particle were getting clearer. In 1962 Lederman, Schwartz, and Steinberg had proved the existence of a neutrino associated to the interactions of the muon, the muon neutrino ν_μ [12], and when the tau was discovered at SLAC [13], it was immediately postulated the existence of a third neutrino, ν_τ (finally discovered in the DONUT experiment, in 2000 [14]). The interactions of these three families of leptons, electron, muon, and tau, and their corresponding neutrinos, were understood in the context of Fermi's theory, but their fundamental description was provided by Steven Weinberg's seminal paper [15], where weak interactions are mediated by three heavy spin-1 particles, the $W^\pm$ and the Z.

Most of the experiments targeting the detection of extraterrestrial neutrinos, the *neutrino telescopes*, are built underground or in sites screened by thick layers of rock, such as mountains or mines. This is because the Earth is constantly hit by a flux of extraterrestrial particles, the *cosmic rays* (CRs), that interacting with the atmosphere can initiate chain reactions of scattering events, called *particle showers*. The secondary particles stemming from CRs interactions with the atmosphere are one of the main sources of background in particle physics experiments, as they produce a flux of muons and neutrinos that survive to the ground. These muons need to go through ~ 1 km of dirt for their flux to be significantly attenuated, while neutrinos interact hardly ever and, depending on their energies, can even traverse the Earth unbothered.

Parallel to the experimental effort to understand the flux of ν_e emitted from the Sun, there was a whole industry working to characterize these neutrinos, dubbed "atmospheric". Atmospheric neutrinos have GeV-scale and are produced in the decay of the muons and the charged pions stemming from CRs interactions with the atmosphere, as $\pi^- \to \mu + \bar{\nu}_\mu$ and $\mu \to e + \bar{\nu}_e + \nu_\mu$ (and their charge-conjugated processes).

Atmospheric ν_e, ν_μ, and their antineutrinos, are detected using huge tanks of water instrumented with photomultiplier tubes. These experiments look for the light produced by neutrino interactions. Indeed, the collision of a neutrino with a nucleon can produce its corresponding charged lepton (this is called a "charged-current" interaction). If this lepton has a speed larger than the speed of light of the medium in which it propagates, it emits a cone of light peaked in the near-ultraviolet band, called Cherenkov light.

Atmospheric neutrinos provided an additional piece of the puzzle when the results of the Super-Kamiokande experiment, in the Kamioka mine in Japan, showed evidence of the non-conservation of neutrino flavors [16]. The experiment was able to discriminate the arrival direction, based on the arrival time of the Cherenkov light, and the interactions of ν_e from those of ν_μ, since they produce light cones with different shapes. These neutrinos are expected to be produced with the same properties around the globe, but to reach the detector they need to travel different distances. Fig. 1.2 [17] shows the results of Super-Kamiokande: up-going neutrinos, traversing the Earth's diameter, have a different ratio of ν_e to ν_μ compared to those with down-going directions.

Eventually, Super-Kamiokande was also able to detect neutrinos with lower energies, in particular solar neutrinos. The results [18] were consistent with the discrepancies of the previous experiments, but the extension of Cherenkov techniques to the MeV range paved the way for the final resolution of the 35-year-old solar neutrino problem, which happened with the Sudbury Neutrino Observatory (SNO).

SNO was a Cherenkov experiment in Canada, deploying a large tank of hyperpure heavy water, *i.e.*, with deuterium D instead of hydrogen-1, H. The presence of deuterium allowed three detection channels: the charged-current of electron neutrinos, $\nu_e + \mathrm{D} \to p + p + e^-$, the neutral-current interactions of neutrinos of any flavor x, $\nu_x + \mathrm{D} \to p + n + \nu_x$, and their elastic scattering on atomic electrons, $\nu_x + e^- \to \nu_x + e^-$. The possibility to detect a flavor-specific channel and the overall all-flavor flux of solar neutrinos with two independent flavor-blind channels allowed to measure the ratio of ν_e in the total flux. The results of SNO on solar neutrinos [19] showed that, even though solar neutrinos are produced as ν_e, only a fraction of them maintain this flavor upon detection on Earth. All the results on solar neutrinos mentioned so far are summarized in Fig. 1.3 [20].

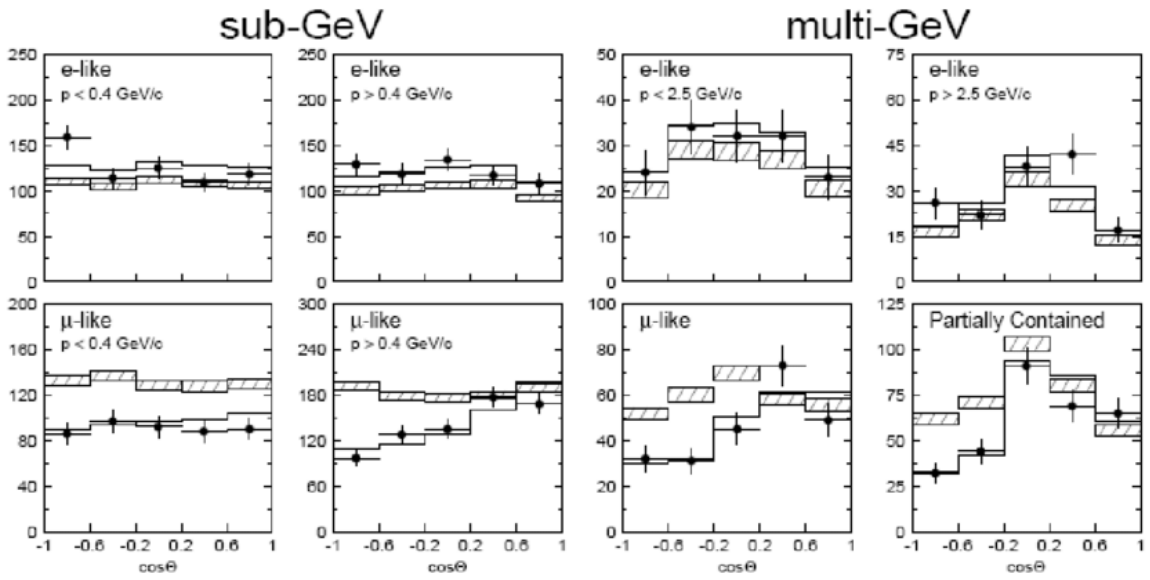

Figure 1.2: **Atmospheric neutrinos measured by Super-Kamiokande.** *Events are grouped according to their flavor and energy, and plotted against the cosine of the zenith angle, θ. Points with error bars are data, hatched boxes are Monte-Carlo simulations without oscillations, solid line are Monte-Carlo simulations using best-fitted oscillation effects. Figure taken from Ref. [17].*

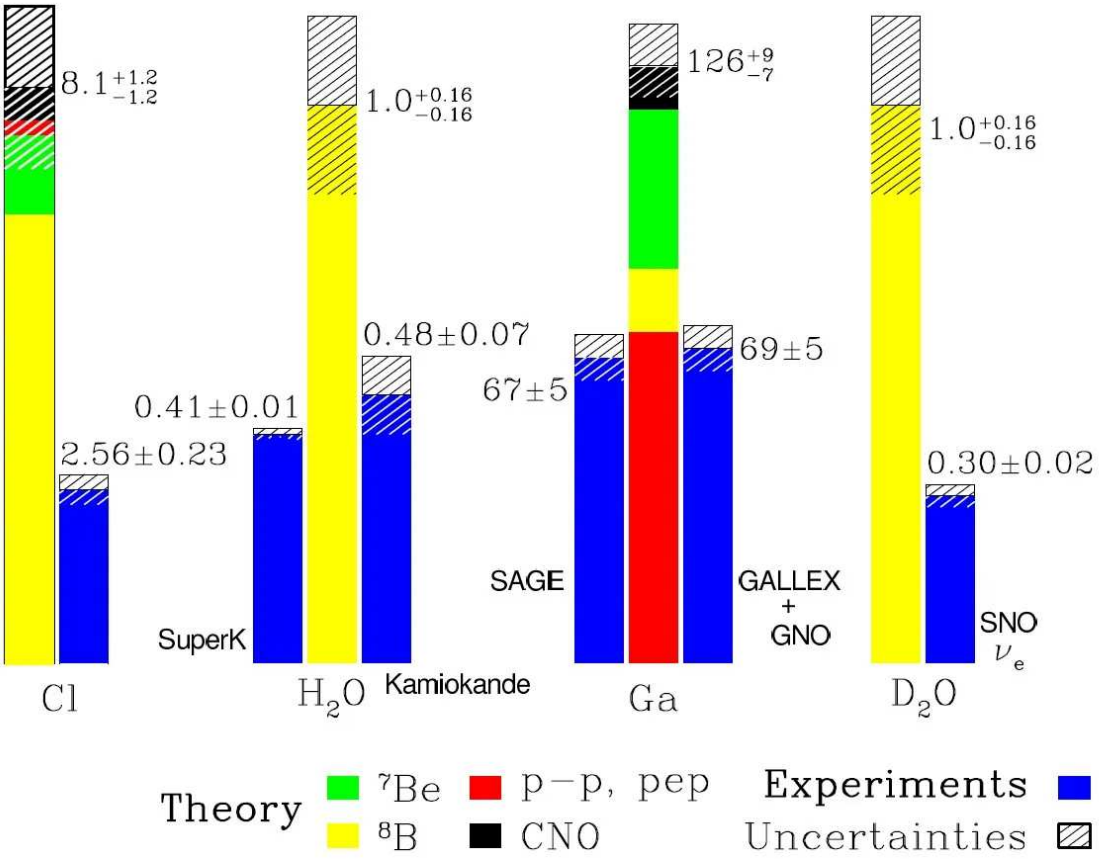

Figure 1.3: **Theoretical predictions and measurements of the flux of solar neutrinos.** *For each experiment, the flux of solar neutrinos from different reactions, computed with the Standard Solar Model (SSM), is compared to the experimental results (in blue). Figure taken from Ref. [20], first shown in Ref. [21].*

This resolution of the solar neutrino problem confirmed what Super-Kamiokande proved for atmospheric neutrinos: the irrefutable presence of new physics, leading to flavor violation in the neutrino sector that depends on their energy, initial flavor and traversed distance. Further experiments using neutrinos from nuclear reactors and from accelerators brought additional evidence to this idea (see Ref. [22] for a compendium of oscillation results). Today, we understand all these data within the theory of neutrino oscillations, which is next introduced and discussed.

1.3 Theory of neutrino oscillations

This section presents the formalism of neutrino oscillations, for which a neutrino produced with flavor α is measured with a flavor β that can be different ($\alpha, \beta = e, \mu, \tau$), and shows why it implies that neutrinos are massive particles. As stated in the last section, this theory can explain why the fraction of ν_e that we measure in the flux of solar neutrino is not one, as found by SNO, and why the ratio of ν_e to ν_μ for atmospheric neutrinos is not constant, in energy nor in arrival direction, as found by Super-Kamiokande.

The idea of neutrino oscillations had been proposed by Bruno Pontecorvo [23] already in 1958, when he suggested the possibility of $\nu \longleftrightarrow \bar{\nu}$ oscillations in analogy of those of meson-antimeson, and extended in 1967 [24] to two-flavors $\nu_e \longleftrightarrow \nu_\mu$ oscillations. In this latter paper he considered the violation of lepton number and the existence of a mass, which were later confirmed experimentally. Today we know there are three families, or *flavors*, of neutrinos, associated to the three charged leptons.

There could be in principle additional neutrinos, yet undiscovered. However, from the total decay width of the Z boson measured at the LEP experiment [25], as well from astrophysical studies of Big Bang nucleosynthesis and the cosmic microwave background (see, *e.g.*, [26]), we know that the number of *active* neutrino families, *i.e.*, those interacting with Standard Model particles, is exactly three, at least up to the energy scales at which the Standard Model has been tested.

We organize them in a three-dimensional flavor multiplet of neutrino fields ν_α ($\alpha = e, \mu, \tau$), which are eigenstates of the weak interactions. Neutrinos are massless in the Standard Model, but if we assume the existence of a non-zero mass, then the three mass eigenstates, denoted by ν_i ($i = 1, 2, 3$) and with masses m_i, will be in general rotated with respect to the flavor basis, *i.e.*,

$$\nu_\alpha = \sum_i U_{\alpha i}\, \nu_i \ .$$

The unitary matrix U, called the PMNS (Pontecorvo-Maki-Nakagawa-Sakata) lepton mixing matrix, can be parameterized by three mixing angles, $\theta_{12}, \theta_{23}, \theta_{13}$, and a CP-violating phase, δ. These parameters are measured in experiments using neutrinos from different sources, and it is usually given in the form

$$U = \begin{pmatrix} 1 & 0 & 0 \\ 0 & \cos\theta_{23} & \sin\theta_{23} \\ 0 & -\sin\theta_{23} & \cos\theta_{23} \end{pmatrix} \begin{pmatrix} \cos\theta_{13} & 0 & \sin\theta_{13} e^{-i\delta} \\ 0 & 1 & 0 \\ -\sin\theta_{13} e^{+i\delta} & 0 & \cos\theta_{13} \end{pmatrix} \begin{pmatrix} \cos\theta_{12} & \sin\theta_{12} & 0 \\ -\sin\theta_{12} & \cos\theta_{12} & 0 \\ 0 & 0 & 1 \end{pmatrix} \ ,$$

which is made up of the terms relevant for the oscillations of atmospheric neutrinos (first rotation matrix), reactor neutrinos (second) and solar neutrinos (third).

If we consider a pure state of flavor $|\nu_\alpha\rangle$, this is produced as a coherent superposition of the three mass eigenstates $|\nu_i\rangle$. Quantum fields destroy one-particle states and create one-antiparticle states, so we have

$$|\nu_\alpha\rangle = \sum_i U^*_{\alpha i} \, |\nu_i\rangle \ .$$

In order to relate the PMNS parameters to measurable quantities, we compute the probability for a pure state in the flavor eigenstate $|\nu_\alpha\rangle$, produced at space-time coordinates $(0, \mathbf{0})$, to be found at space-time coordinates $(t, \mathbf{x})$ in the flavor state $|\nu_\beta\rangle$.

States evolve in time via the action of the Hamiltonian operator H, and in space according to the three-momentum operator $\mathbf{P}$. Thus, their evolution is better understood when written in the propagation eigenbasis $|\nu_i\rangle$ (*i.e.*, the one that diagonalizes the Hamiltonian operator). In that case, and assuming natural units where $c = \hbar = 1$, a pure state $|\nu_i\rangle$ evolves in space and time as

$$|\nu_i\,(\mathbf{x}, t)\rangle = e^{i(Ht - \mathbf{P}\cdot\mathbf{x})} \, |\nu_i\rangle = e^{i\left(E^i_\nu t - \mathbf{p}^i\cdot\mathbf{x}\right)} \, |\nu_i\rangle \ ,$$

where $\mathbf{p}^i$ is the 3-momentum of the ν_i and $E^i_\nu = \sqrt{m_i^2 + |\mathbf{p}^i|^2}$ is its total energy. For relativistic particles, in these units, $E \approx |\mathbf{p}|$ and $t \approx L$, where L is the traversed distance, the *baseline*. Thus, for neutrinos we can approximate $E^i_\nu \, t - \mathbf{p}^i \cdot \mathbf{x} \approx (E^i_\nu - |\mathbf{p}^i|)L \approx \frac{m_i^2}{2E^i_\nu}$.

First, we consider the simplest case of free propagation in vacuum, for which the operator governing the space-time evolution is the free Hamiltonian H_0. In this case, the propagation eigenstates are the mass eigenstates, and the rotation with respect to the flavor basis is given by the PMNS matrix U. The oscillation probability is computed, after some algebra, as

$$\begin{aligned} \mathrm{P}_{\alpha\to\beta}\,(\mathbf{x}, t) &= |\langle \nu_\beta(\mathbf{x}, t) \,|\, \nu_\alpha\rangle|^{\ 2} = \\ &= \sum_i |U_{\beta i}|^2 \ |U_{\alpha i}|^2 + \sum_{i\neq k} U_{\beta i} U^*_{\alpha i} U^*_{\beta k} U_{\alpha k} e^{i\left(E^i_\nu t - \mathbf{p}^i\cdot\mathbf{x}\right)} e^{-i\left(E^k_\nu t - \mathbf{p}^k\cdot\mathbf{x}\right)} \ . \end{aligned} \tag{1.1}$$

This probability is given by the sum of a constant term, due to the relative rotation of the flavor and propagation eigenstates, and an oscillating term, due to the different phase velocities of the three mass eigenstates.

Using the relativistic approximation, and neglecting higher-order differences in the energies $E^i_\nu \simeq E_\nu$, we write explicitly the oscillation probability for a neutrino of energy E_ν, traversing a baseline L, as

$$\mathrm{P}_{\alpha\to\beta}\,(L, E_\nu) = \sum_i |U_{\beta i}|^2 \ |U_{\alpha i}|^2 + \sum_{i\neq k} U_{\beta i} U^*_{\alpha i} U^*_{\beta k} U_{\alpha k} e^{i\frac{m_i^2 - m_k^2}{2E_\nu} L} \ . \tag{1.2}$$

As we mentioned before, the experimental evidences for neutrino oscillations implies the existence of a mass for neutrinos (thus, of physics beyond the Standard Model!) and Eq. (1.2) shows why: a mass term for neutrinos allows to rotate non-trivially the two basis (yielding a unitary matrix U different from the identity), and it enters explicitly in the oscillating term via $\Delta m^2_{ij} \equiv m_i^2 - m_j^2$. Note that there are only two independent Δm^2_{ij}, and having measured $\Delta m^2_{ij} \neq 0$ requires that at least two of the three mass eigenstates should be massive (one could be massless).

Performing oscillation experiments over different baselines and energy ranges it has been possible to measure the values of the PMNS parameters and the mass differences Δm^2_{ij} [27, 28]. Yet, it's still uncertain what is the hierarchy of the masses m_i: future experiments will use oscillation data to clarify whether the correct mass hierarchy is $m_1 < m_2 < m_3$ (the normal ordering) or $m_3 < m_1 < m_2$ (the inverted ordering).

Oscillation experiments are sensitive only to the squared-mass differences, so they cannot probe the overall mass scale of neutrinos. At present, the strongest upper limit on neutrino mass comes from cosmology $\sum_i m_i < 0.12$ eV [29], but there are also results from laboratory experiments, measuring with high precision the end-point energy of the β spectrum of tritium: the KATRIN experiment set the bound $m_{\nu_e} < 0.8$ eV [30].

The results presented so far hold for the free propagation of neutrinos in vacuum, in which case the propagation eigenstates are the mass eigenstates (and the matrix that rotates the propagation eigenbasis with respect to the flavor basis is the PMNS matrix U). However, in general, the propagation of neutrinos may receive significant contributions from interaction terms, either from matter effects (this is the case for the Mikheyev–Smirnov–Wolfenstein effect in the Sun [31, 32]) or from beyond-the-Standard-Model (BSM) effects [33]. In these cases, the calculation Eq. (1.2) generalizes to any interaction described by a Hamiltonian H if $|\nu_i\rangle$ are the propagation eigenstates, in general different from the mass eigenstates. Note that in this case the rotation matrix is no longer the PMNS matrix U, which relates the mass and flavor basis, but a different unitary matrix that we denote by $\mathcal{U}$. In general, diagonalizing the Hamiltonian is non-trivial and cannot be done analytically. During this work we will consider also non-standard oscillations induced by BSM physics. In those case, the diagonalization will be performed numerically.

Chapter 2

Neutrino Astrophysics

In Chapter 1, we introduced the main features of neutrinos and the most important mechanisms that generate them: the nuclear processes happening in reactors and in the Sun, and the decay of charged mesons produced in accelerator experiments and in the interactions of cosmic particles with the atmosphere. This latter process is a consequence of the existence of a flux of CRs, which was discovered by Victor Hess in 1912 [34].

Since then, numerous measurements of CRs have been performed, using several techniques and over wide energy ranges. Our current knowledge of this flux, shown in Fig. 2.1 [35], is that the flux of CRs follows a power law in energy, with multiple spectral breaks, spanning over 10 decades in energy, going as far as the ZeV. A fraction of these cosmic rays arrives on Earth with extreme energies, of EeV-scale. When these ultra-high-energy cosmic rays (UHECRs) interact with a proton in the atmosphere they can reach center-of-mass energies $\sqrt{s}$ orders of magnitude larger than those of the Large Hadron Collider (LHC), which is capped at $\sqrt{s} = 14$ TeV.

The observation of this flux implies the existence of powerful astrophysical sources, capable of accelerating particles up to these extreme energies. The nature of such sources and the physics behind the acceleration of cosmic rays are still debated (see, *e.g.*, [37, 38] for a review). This is partially due to the fact that CRs are charged particles, so during their propagation they are bent by Galactic and extragalactic magnetic fields; when they are detected, it is not possible to use their incoming direction to point back at the astrophysical object that produced them.

Hope is not lost, though, since during the acceleration process multiple radiative processes and interactions take place, generating secondary particles that may better point back at their sources [39, 40]. If the particles accelerated are leptons they can emit photons over a broad band of frequencies, depending on the particle energies and properties of the sources. Instead, if the particles accelerated are hadrons (protons or heavier nuclei), also high-energy neutrinos are produced. We focus on the case of hadronic cosmic accelerators. The photons and neutrinos stem from the pions produced in the collisions of the accelerated hadronic CRs with ambient matter or radiation fields, in reactions such as

$$p + \text{nucleus} \to \pi^{(\pm,0)} + X$$
$$p + \gamma \to \Delta^+ \to \begin{cases} \pi^0 + p \\ n + \pi^\pm \end{cases} .$$

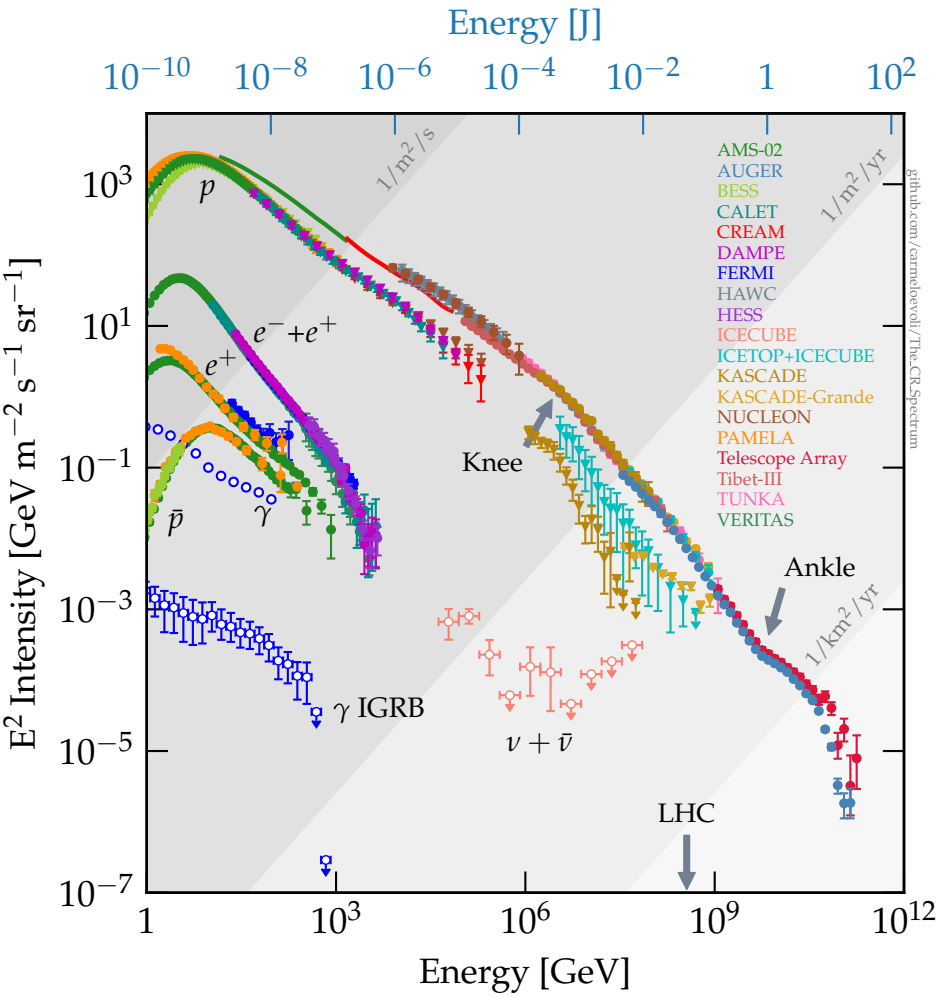

Figure 2.1: **Flux of cosmic rays.** *The flux extends over many decades in energy. At lower energies the experiments are performed on satellites, at higher energies they measure from Earth the particle showers initiated by cosmic rays hitting the atmosphere. Data and references of the plot are listed in [36].*

These pions promptly decay as $\pi^0 \to \gamma\gamma$ and $\pi^\pm \to \mu\nu_\mu \to e\nu_\mu\nu_e\nu_\mu$, with typical energies $E_\nu \sim E_p/20$ and $E_\gamma \sim E_p/10$.

Being neutral, photons and neutrinos travel straight, not deflected by magnetic fields. High-energy photons can rapidly lose their energy via different processes, depending on the environment, and above the TeV their flux is suppressed due to pair production with background photon fields [41]. On the contrary, neutrinos interact feebly with ordinary matter and are unaffected by cosmic photon backgrounds, so they reach us with nearly the same energy with which they were produced, and point back to their sources. Later we elaborate on our current knowledge on these sources, but for now it is enough to state that if an astrophysical object accelerates hadrons, it will produce a flux of neutrinos. Having observed CRs with high energies, a flux of secondary high-energy neutrinos is expected, though its magnitude depends on the properties of the sources making it.

As we saw in the last chapter, neutrino interactions are weak, and the only hope to detect them is to instrument a volume large enough to produce enough events, given

the flux. Then, an estimate of the flux was necessary in order to envision a suitable detector.

In 1998, Eli Waxman and John Bahcall computed an upper bound on the flux of high-energy neutrinos [42]. Using the cosmic-ray measurements of the time and relying on assumptions on the size of the unknown sources of UHECRs, they found that the energy flux of neutrinos produced by $p-\gamma$ or $p-p$ interactions at their source should be

$$E_\nu^2 \Phi_\nu < 2 \times 10^{-8} \text{ GeV cm}^{-2} \text{ s}^{-1} \text{ sr}^{-1} .$$

The Waxman-Bahcall bound has been an important benchmark for the flux in the years to come. Moreover, it implied that the flux of high-energy cosmic neutrinos actually required a $\gtrsim \text{km}^3$ scale detector in order to be discovered.

As we saw for Super-Kamiokande, a competitive idea for an experiment of such dimensions consist in instrumenting a a large volume of transparent medium with photomultiplier tubes and searching for the Cherenkov light produced in the interactions. A comparison is needed though: the water tank of Super-Kamiokande has a volume of about $50,000$ m^3, almost ten thousand times smaller than the one necessary to see a flux close to the Waxman-Bahcall bound!

How can we build such a huge detector? First, a large volume of naturally available medium, transparent to light in the UV band, must be available, and ice and water are the best candidates. New detectors of increasing size were constructed in lakes and in the ice (see [43] for a historic review), growing the experience in the field that eventually led to complete, in 2011, the first experiment able to challenge the Waxman-Bahcall bound: the IceCube Neutrino Observatory.

In 2013 the IceCube experiment discovered a diffuse flux of high-energy astrophysical neutrinos, confirming its existence and measuring a flux very close to the Waxman-Bahcall bound. Given the utmost importance of IceCube in our current understanding of neutrino astrophysics, we first review the design and the physics of IceCube, and then discuss some of its major discoveries.

2.1 The IceCube Neutrino Observatory

IceCube [44] is a neutrino telescope located near the Amundsen-Scott South Pole Station, in Antarctica. It instruments a cubic-kilometer of pure ice with more than 5000 digital optical modules (DOMs) deployed in vertical strings (see Fig. 2.2). Each DOM contains a photomultiplier tube, and since light has an attenuation length of $\mathcal{O}(10-100 \text{ m})$ in the ice, they can detect the Cherenkov light emitted by relativistic charged particles propagating in the medium. In particular, IceCube can detect the secondary particles of neutrino interactions.

A neutrino (or an antineutrino) of flavor α can undergo deep inelastic scattering with one of the quarks or gluons inside a proton or a neutron of a nucleus N, via charged-current (CC) or neutral current (NC) interactions, as

$$\begin{aligned} \nu_\alpha + N &\to \alpha + X \quad \text{(CC)} , \\ \nu_\alpha + N &\to \nu_\alpha + X \quad \text{(NC)} . \end{aligned}$$

The products of the scattering, X, and the charged leptons α, are detected via Cherenkov light. Analogous reactions hold for antineutrinos: here we will refer indifferently to

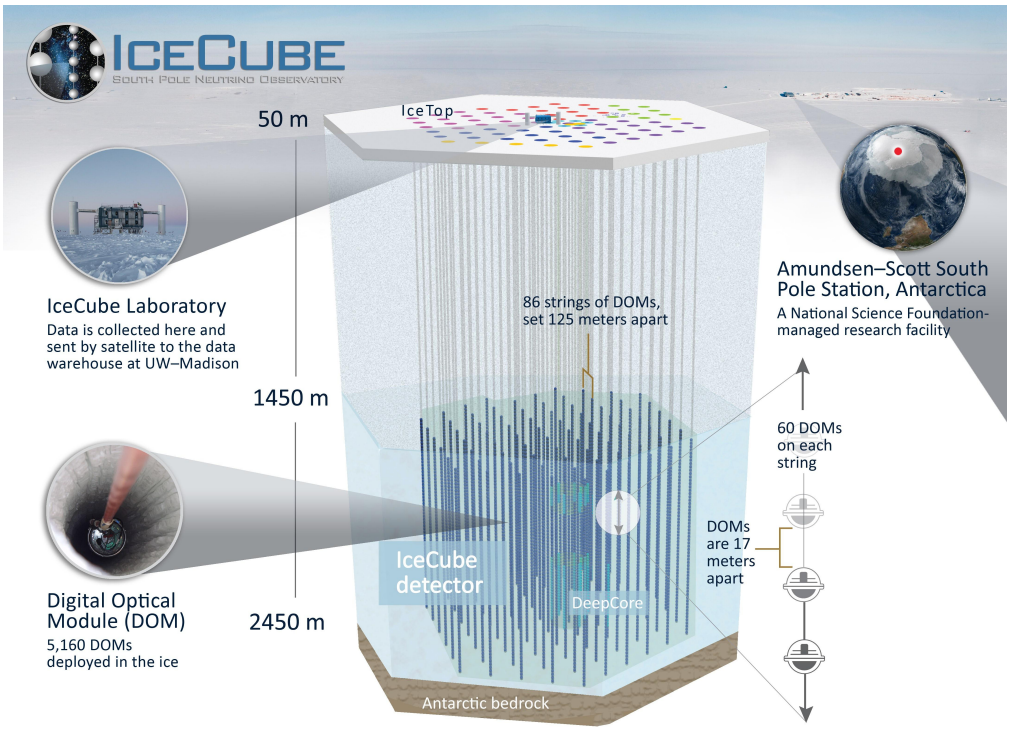

Figure 2.2: **The IceCube Neutrino Observatory.** *Scheme of the experiment. Figure taken from Ref. [46].*

both of them as neutrinos, since they are indistinguishable in the detector (with the sole exception of the Glashow resonance, where a $\bar{\nu}_e$ interacts with an atomic electron and produces an on-shell W boson [45]). Combining the measurement of the number of photons collected by each DOM and their arrival time, it is possible to infer the direction of the charged particle and its energy. The large momentum transfer of these interactions ensures that the directions of secondary particles are closely aligned with the neutrino direction, enabling to reconstruct the latter.

High-energy neutrinos produce two different event topologies in IceCube: *tracks* and *cascades*. Tracks are produced when a muon neutrino undergoes a CC interaction, generating a muon that traverses a long distance before decaying or scattering again; these events have an angular resolution $< 1^\circ$, but since only a fraction of the muon energy is deposited in the detector, the neutrino energy is inferred only uncertainly. The situation is different for cascades, *i.e.*, events where the NC interactions of neutrinos of any flavor, as well as the CC interactions of electron neutrinos, produce a particle shower. Due to the high inelasticity of these interactions, almost all the energy of the neutrino is deposited in a small region and results in a nearly spherical event. The charged part of the shower emits Cherenkov radiation, and the energy of the neutrino is reconstructed with $\sim 15\%$ precision, but due to the broad distribution of the shower, the angular resolution is poorer, of $\mathcal{O}(10^\circ)$.

Another important event topology is the CC interaction of tau neutrinos, where the resulting tau lepton decays in a different vertex and creates a typical *double bang* signature [47], with two separate cascades. The first ν_τ events of this kind have been recently discovered by IceCube [48, 49].

The biggest issue in detecting astrophysical neutrinos is the high background of

atmospheric neutrinos and muons that challenges the selection of astrophysical events. IceCube is built 1.5 km underground, so the flux of particles produced by CRs interacting in the atmosphere is damped before arriving to the detector. However, this not hold for atmospheric muons, since they have a significant probability to survive to decay and scattering up to the detector, and atmospheric neutrinos, which can reach unbothered the detector, and interacting produce the same signature of the astrophysical neutrinos IceCube is looking for. To give an idea, IceCube detects every year $\mathcal{O}(10^{11})$ atmospheric muons, $\mathcal{O}(10^5)$ atmospheric neutrinos and only $\mathcal{O}(10)$ astrophysical neutrinos. This demands a thorough characterization of the background, together with specific analysis to select high-purity astrophysical samples out of the multitude of events continuously recorded.
The main criteria to select the candidate astrophysical events are:

- **High-Energy Starting Events (HESE):** these are the events where a neutrino interacts within the detector. An outer layer of DOMs is used as veto to eliminate the events where a ν_μ detected in the fiducial volume of the detector is accompanied by a muon co-detected in the veto, which would reveal the atmospheric origin of the neutrino (since the muons that accompany astrophysical ν_μ have longed ago decayed).

- **Throughgoing tracks:** events whose reconstructed direction points to the Northern Hemisphere. The background from atmospheric muons is nearly completely suppressed due to absorption while traversing the Earth. On the other hand, since the cross section for neutrino-nucleon scattering increases with energy, the flux of high-energy up-going neutrinos is partially suppressed as well.

2.1.1 Discovery of high-energy astrophysical neutrinos

Having discussed the physics behind the events detected at IceCube, we proceed to review the main scientific results of this experiment.

As we anticipated, IceCube has been the first detector sensitive to the Waxman-Bahcall benchmark flux, and the one that discovered the flux of high-energy astrophysical neutrinos that we discussed so far. The first step that led to the discovery was the first observation of neutrino events with PeV-scale energies [50]. In 2013, two years after IceCube started operating in full-regime, the Collaboration reported the detection of two neutrino events with energies of about 1 PeV, the highest energy ever observed for a neutrino. The two events, fully-contained cascades, were incompatible at 3σ with atmospheric background-only hypothesis, and motivated a more in-depth all-sky search.

Analyzing the first two years of IceCube HESE, the Collaboration found a 4σ evidence for the existence of a diffuse flux of high-energy extraterrestrial neutrinos [51], yielding a number of high-energy events that could not be explained by the sole atmospheric background. Analyzing an additional year of data containing events in the 100 TeV–PeV range, the significance of this result increased to 5.7σ [52], larger than the 5σ necessary to claim a discovery.

In the subsequent years additional analysis of IceCube HESE [53] and up-going muon tracks [54], with improved statistics and more refined models, consolidated this

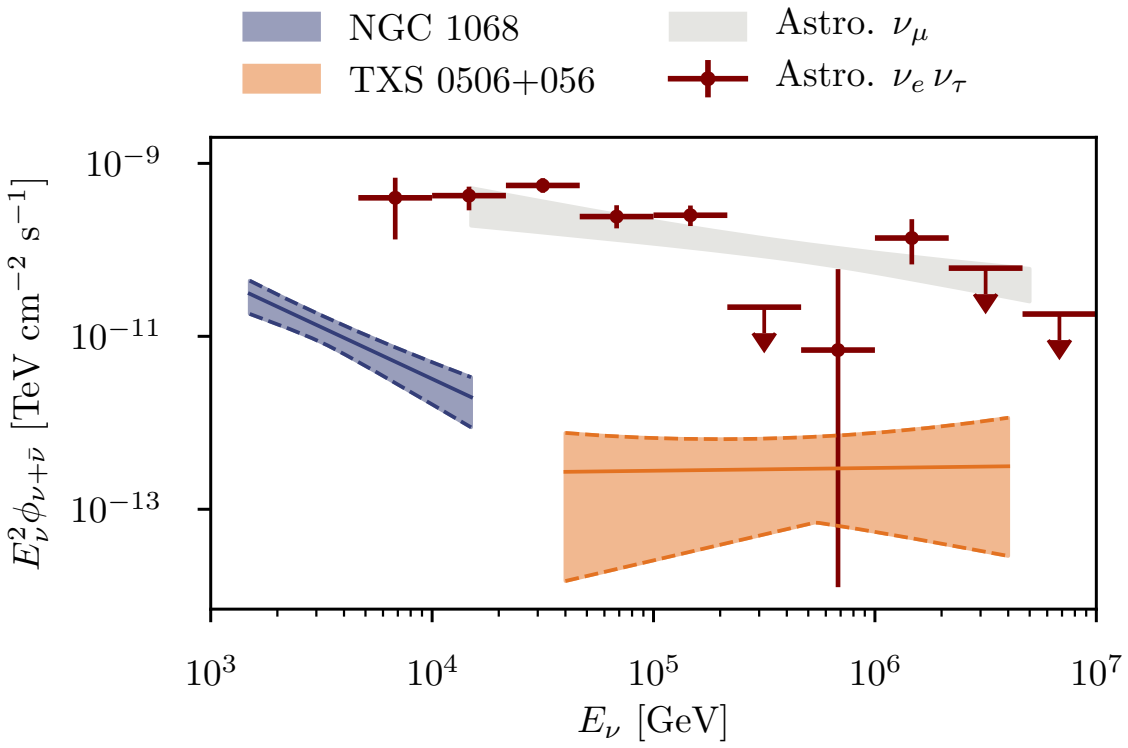

Figure 2.3: **Flux of high-energy astrophysical neutrinos measured by IceCube.** *Comparison between the total diffuse flux of ν_μ [54] and $\nu_e+\nu_\tau$ [56] and the point-source fluxes measured for NGC 1068 [55] and TXS 0506+056 [57]. Fluxes are given for a single flavor of neutrinos and anti-neutrinos assuming equal flavor ratio. The bands provide simultaneous coverage at* 68% *C.L.. Figure taken from Ref. [55].*

discovery. Fig. 2.3 [55] shows diffuse flux of high-energy astrophysical neutrinos measured by IceCube and compares them to two point-sources discovered in the recent years (more on this later).

2.2 Astrophysical sources of high-energy neutrinos

Today, the existence of a diffuse flux of high-energy astrophysical neutrinos is a well-established fact. The angular distribution of the events is compatible with an isotropic distribution of sources, and this hints that they are very far, probably extra-galactic. However, it is still unclear what are the sources of these neutrinos: how do they work and how can we identify them?

As we stated earlier, a flux of high-energy neutrinos is expected from the interactions of UHECRs. Thus, searches for neutrino sources focus on objects that are candidate UHECR accelerators. The acceleration mechanism at work in these sources is still an open question, though the dominant model is the diffusive shock acceleration [40], in which particles are repeatedly swept by shock waves.

From measurements of the electromagnetic radiation over different wavelengths, different candidates in which this process could be at work have been identified, including:

- **Gamma ray bursts (GRBs):** these are luminous, but short flashes of gamma rays generated in especially energetic supernovae or in compact-object mergers (see Ref. [58] for a review).
- **Active galaxies:** these are galaxies that host an active galactic nucleus (AGN), a compact region from which radiation is emitted across the electromagnetic spectrum. The dominant theory is that an AGN consists of a supermassive black hole accreting and heating gas and dust. The observed characteristics of an AGN depend on the viewing angle [59]. In some cases, the AGN can launch a strong, narrow jet of accelerated plasma. If such a jet is oriented close to the line of sight, the AGN is called a blazar.
- **Tidal disruption events (TDEs):** processes in which solar-mass stars are ripped apart by tidal forces when they get close to a supermassive black hole. The accretion of the stellar matter on this black hole leads to the emission of energetic radiation, though for shorter periods compared to AGNs (see, *e.g.*, [60] for a review).

To proceed in this search, further assumptions are necessary, due to the overwhelming number of data and potential sources. Catalog-based searches for sources of neutrinos look for neutrinos whose incoming directions coincide with the positions of known astrophysical objects, selected *a priori* among the surveys collected by different experiments. The most suitable events for these point-source searches are muon tracks, since they have the best angular resolution.

The first identification of an astrophysical neutrino source was in 2017, when a neutrino event was observed in coincidence, in direction and time, with a gamma-ray flare from the blazar TXS 0506+056 [57]. This was possible thanks to the real time alert system of IceCube [61], that send and receive warnings to a community of telescopes when triggered by interesting events: this allows to perform multi-messenger association and follow-up observations. Analyzing the neutrino events recorded in ten years in the direction of the blazar, the Collaboration found an excess of events, 3.5σ away from the background hypothesis.

Further evidence supporting AGNs as neutrino sources came when the Collaboration announced that an excess of events was found compatible at 4.2σ with the position of a close AGN, NGC 1068 [55]. These analysis were performed using up-going events to reduce the atmospheric background. The point-source fluxes measured by IceCube for NGC 1068 and TXS 0506+056 are shown in Fig. 2.3.

Besides these two AGNs, the most recent important result regarding neutrino sources have been the discovery of neutrinos from the Galactic Plane [62]. The drawback of using up-going events is that only data from the Northern Hemisphere. Data from the Southern Hemisphere, and in particular from the center of our Galaxy, suffer heavy background from atmospheric muons. The Galactic Plane has been considered a guaranteed source of neutrinos since the observation of gamma-ray signatures from π^0 decay, but the search for Galactic neutrinos was challenged by the large background. Using machine learning algorithms the Collaboration was able to look for a neutrino emission in the region of the Plane in which γ rays from π^0 decay have been detected. The analysis showed a 4.2σ evidence for a flux of neutrinos from the Galactic Plane.

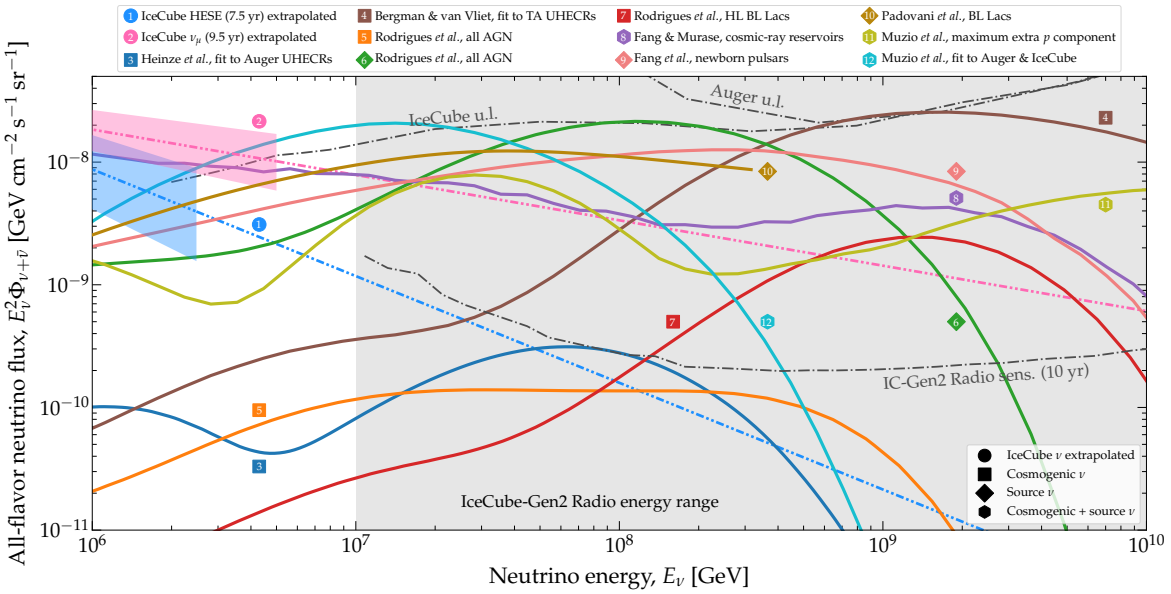

Figure 2.4: **Benchmark diffuse ultra-high-energy neutrino flux models.** *Landscape of the theoretical predictions in the literature [65, 66, 67, 68, 69, 70, 71, 53, 72, 73]. Figure taken from Ref. [64].*

2.3 Ultra-high-energy neutrinos

Already in 1969, Berezinsky and Zatsepin noted that a flux of neutrinos with energies in excess of 100 PeV should be expected, from the $p-\gamma$ interactions of UHECRs with the cosmic microwave background [63]. These ultra-high-energy (UHE) neutrinos have been searched with different techniques, but they have never been detected.

From our current knowledge on UHECRs and the theoretical models on their candidate sources we expect the existence of a flux of UHE neutrinos not only from the interactions of UHECRs during their propagation (*cosmogenic neutrinos*), but also possibly from interaction inside their sources or close to them, with ambient matter or radiation. We refer to neutrinos produced at source as *source neutrinos*, and we show in Fig. 2.4 [64] the current theoretical picture of source and cosmogenic UHE neutrinos from a variety of theoretical flux predictions. Our goal here is not to examine and assess the competing theoretical predictions of the UHECR flux, but simply to take them as representative of the space of possibilities. Later, we will use a few of them as realistic astrophysical inputs in our analysis.

A population of UHE neutrinos is *guaranteed* to exist from general grounds, as a consequence of UHECRs. However, the breadth of the theoretical possibilities is still wide, due to the uncertainty on the energy spectrum of UHECRs, their mass composition, and properties of the UHECR sources such as their abundance at different redshifts. As we will see in the next chapter, there is an important effort ongoing from the experimental community: new experiments, currently under planning, are targeting the UHE range and may lead us to discover UHE neutrinos in the next decade.

Chapter 3

Radio-detection of ultra-high-energy neutrinos

Cosmic neutrinos with energies in the TeV–PeV range are regularly detected by IceCube, by means of the Cherenkov light radiated by the charged products of their interactions. In principle, these optical techniques are able to detect neutrinos of higher energies, but no neutrino above 10 PeV has ever been observed by IceCube, allowing to set an upper bound on the flux of UHE neutrinos [74]. Given this result, how can we proceed in order to detect the long-sought UHE neutrinos?

The most natural solution would be to expand IceCube, enlarging the active volume with additional strings of DOMs. Unfortunately, reaching the sensitivity required by theoretical models in this way is cost-prohibitive. Thus, a change of paradigm from the well-established optical techniques is required in experimental neutrino astrophysics.

In light of this, in the upcoming decade a new generation of neutrino telescopes, currently under planning, will use radio techniques to push the sensitivity to fluxes of neutrinos in the ultra-high energy range to unprecedented levels. These experiments will rely on arrays of radio antennas to detect the particle showers initiated by neutrino-nucleon interactions and developing in-ice (the radio array of IceCube-Gen2 and RNO-G) or in air (GRAND). Indeed, thanks to the longer attenuation length of radio waves, of $\mathcal{O}(1\text{ km})$ in ice and $\mathcal{O}(10\text{ km})$ in air, it will be possible to detect radio signals even with a sparse array of antennas. This feature, together with the relative affordability and the endurance of the antennas, will allow to instrument large surfaces, yielding sensitivity to very low fluxes of neutrinos.

In this chapter we review the physics behind these experiments, presenting the design and the main features of in-ice and surface telescopes and showing their projected sensitivities.

3.1 Radio signatures of particle showers

When high-energy particles interact with a target, usually a nucleon, they start a chain of reactions that generates a particle shower. The size of the shower is proportional to the energy of the particle that initiated it. For UHECRs, because they are too rare to detect directly, we detect them instead via the emission from the extensive air showers that they initiate upon by their interaction in the atmosphere. The development of the shower produces different effects that can be observed: a cone of

Cherenkov light, fluorescence light, and a population of surviving muons that can be detected on ground using Cherenkov water tanks, scintillators or other surface detectors. Observing all these features requires different instruments, thus the state of the art observatories of particle showers, the Pierre Auger Observatory, Telescope Array and the Large High Altitude Air Shower Observatory (LHAASO) are multipurpose experiments, instrumenting large surfaces with water tanks, scintillators, air imaging Cherenkov telescopes, and fluorescence telescopes.

If the particle generating the shower is sufficiently energetic, the development of the shower can also generate a nanosecond-long pulse in the radio band. This is due to two different phenomena, that are always at work but whose relative importance depends on the medium in which the cascade propagates: the Askaryan effect and the geomagnetic effect.

The Askaryan effect is the coherent radio emission generated by the accretion of negative charges during the shower development. Indeed, while the chain of reactions that generates the shower takes place, electrons and positrons are produced. Positrons annihilate on atomic electrons, leading to a charge unbalance that evolves with time, emitting radio waves. This effect is dominant in dense environment, and is the signal searched for in-ice detectors.

The geomagnetic effect, instead, is the emission of radio waves due to the separation of particles of opposite charges moving in the Earth's magnetic field. The charge anisotropy behaves as a time-varying electric current, radiating waves in the radio band. The geomagnetic effect is dominant for showers propagating in air, where the electron density is smaller and the annihilation is less efficient.
In Figure 3.1 [75] the two effects are shown and compared.

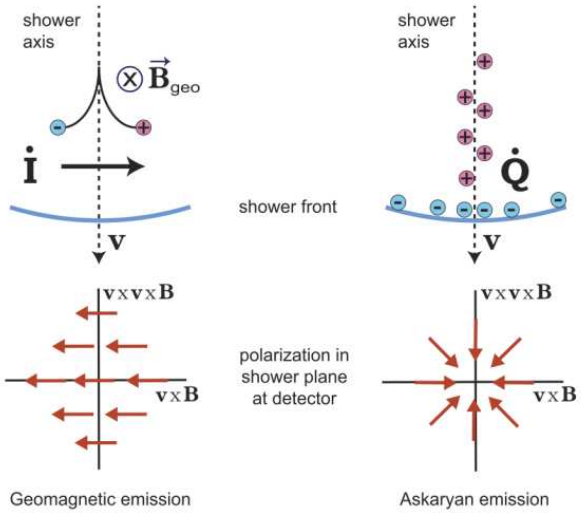

Figure 3.1: **Radio emission from particle showers.** *Figure taken from Ref. [75].*

In summary, the particle showers induced by the most energetic particles, in particular UHE neutrinos, emit an additional observable signature, this time in the radio band. In the following we present the techniques to detect the radio pulses from showers developing in the ice and in the air, and their implementation in the UHE neutrino telescopes under planning.

3.2 In-ice arrays: RNO-G and IceCube-Gen2

A possible way to detect UHE neutrinos is to look for the radio pulses emitted by particle showers initiated by their interactions and propagating in a dense medium. The medium shall be transparent to radio waves in order to detect them, and since the expected fluxes are very low the largest possible surface should be instrumented, meaning that the medium has to be naturally available in large volumes. As for the case of IceCube, the most suitable medium turns out to be the ice.

The UHE neutrino telescopes operating in the ice will cover large surfaces with a sparse array of stations, each operating independently and deploying multiple radio antennas in the ice. The first next-generation UHE neutrino detector will be the Radio Neutrino Observatory in Greenland (RNO-G [76]), currently under construction at Summit Station. RNO-G, whose completion is scheduled for 2026, will bring the operational knowledge gathered from prior ground-based and balloon-based radio neutrino experiments, ARA, ARIANNA, ANITA and RICE [77, 78, 79, 80] one step forward, instrumenting a record number of 35 radio stations. Moreover, the experience collected in its design and calibration will be used to complete and optimize the design of a similar, but larger, detector, the radio array that will be built at the South Pole in the context of the upgrade of IceCube, IceCube-Gen2 [81](2030-2040). The radio array of IceCube-Gen2 will cover a surface of 500 km^2 with $\mathcal{O}(500)$ stations.

RNO-G and the radio array of IceCube-Gen2 will consist of multiple radio stations, similar to the one shown in Fig. 3.2 [81]. Each station will power multiple radio antennas, divided between a shallow component (3 m depth) and a deep component (100 m depth). Some of the antennas in the shallow component will point towards the atmosphere to veto downgoing events, thus reducing the background from cosmic rays via time correlation of the signals.

In Fig. 3.3 a typical in-ice event is shown: a neutrino interacts in the ice and starts a particle shower, whose wavefront propagates to the radio antennas of the station. The refraction of the electromagnetic signal depends on the refractive index of the ice, which changes from the outer layer of soft snow, the firn, to the deeper region of ice, where the pressure makes it denser. This leads to a bending of the signal during its propagation, making an accurate characterization of the optical properties of the ice a necessary condition for calibration.

These experiments will measure the radio signature of the particle shower propagating in the ice, and since these are initiated by neutrinos and antineutrinos of all flavors undergoing CC or NC, UHE neutrino telescopes operating in the ice will be sensitive to the flux of neutrinos of all flavors, though with different interaction probabilities and reconstruction capabilities.

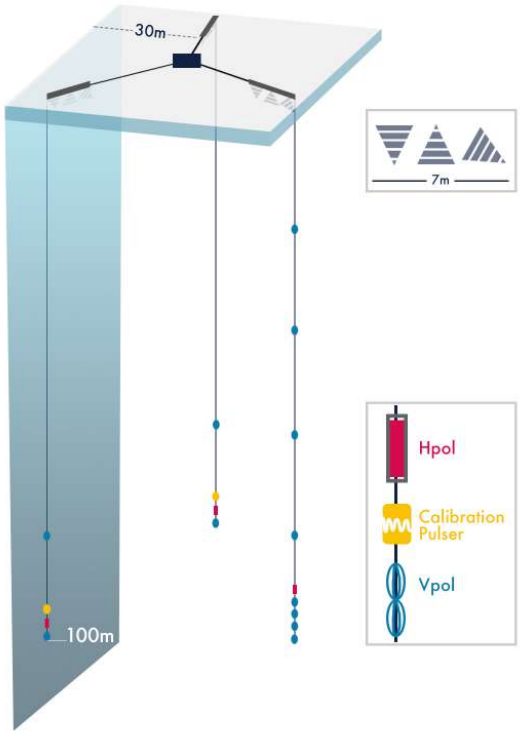

Figure 3.2: **In-ice radio station.** *RNO-G and the radio array of IceCube-Gen2 will deploy multiple in-ice stations similar to this. Figure taken from Ref. [81].*

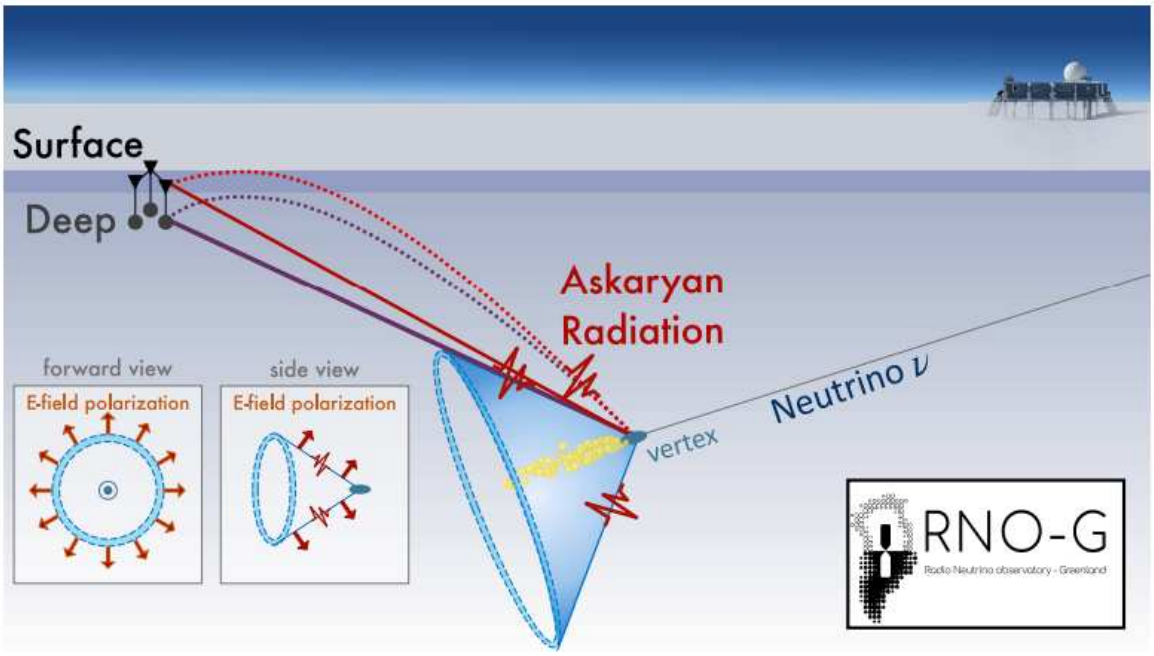

Figure 3.3: **In-ice detection of particle showers.** *Sketch of a neutrino event. Figure taken from Ref. [81].*

3.3 Measuring air showers with GRAND

The radio-detection of extensive air showers (EAS) induced by UHE neutrinos relies on similar techniques, but this time the radio array is distributed above the ground.

These experiments look for Earth-skimming neutrino events, in which a UHE neutrino interacts underground and produces an inclined EAS. As the interaction length of UHE neutrinos is of $\mathcal{O}(100$ km), the Earth is opaque to UHE neutrinos and they are expected to reach the detector only when coming from directions close to the horizon, where the column depth is shorter. Downgoing events will also reach the detector, but from these directions there is a large background of UHECRs that trigger a large background flux of showers.

The larger experiment targeting their discovery with this method will be the Giant Radio Array for Neutrino Detection (GRAND) [82]. The experiment, currently under planning, will instrument large surfaces with arrays of radio antennas. GRAND will consist of clusters of 10,000 antennas each, built in different sites, or *hotspots*. The hotspots will be on mountain slopes, to optimize the detection of inclined showers and exploit the naturally low electromagnetic background, and the additional target for neutrinos brought by the mountain rocks. The construction plan of GRAND is envisioned to be staged, going through three major phases, GRAND10k, GRAND50k and finally the full planned configuration with 200,000 antennas, GRAND200k (2030-2040).

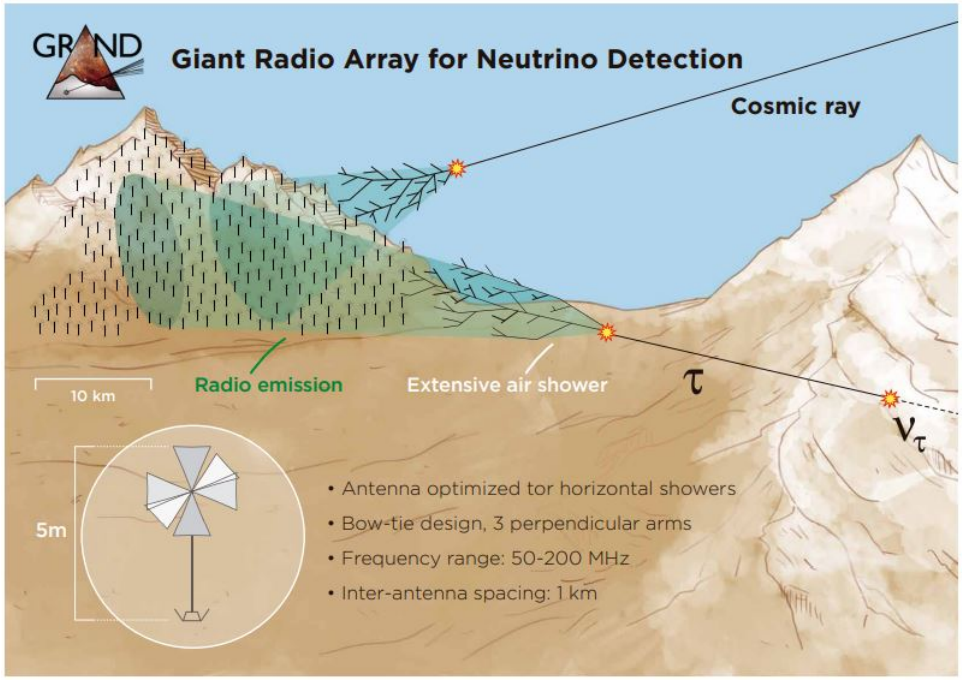

Figure 3.4: **The Giant Radio Array for Neutrino Detection (GRAND):** *a typical event and a background event. Figure taken from Ref. [82].*

Due to the characteristics of the experiment, the main neutrino detection channel in GRAND will consist in a ν_τ CC interaction with a nucleon underground or in the mountain and producing a tau. The tau exits the dense medium and decays after a length of $1 - 10$ km at these energies, inducing a particle shower that, due to

geomagnetic effect, emits a coherent radio pulse that is detected by the antennas. If the UHE neutrino is a ν_e, the electromagnetic cascade stemming from its CC or NC interactions is damped in the dense medium, while if it is a ν_μ the muon stemming from its CC interaction may exit into the air, but the probability for it to decay and start a shower in the field of view of the array is small.

A thorough description of the different interactions and the effects taken into account to simulate the detector response can be found in Ref. [82], but, for our purposes, they key detection aspect is that GRAND will be sensitive mostly to ν_τ and $\bar{\nu}_\tau$. A sketch of a ν_τ event and of a background cosmic ray event, is shown in Fig. 3.4 [82]. The angular resolution of GRAND will be of sub-degree level, meaning that a significant part of the background, coming from cosmic rays interacting in the atmosphere, will be removed in the analysis by quality cuts on the arrival direction.

3.4 Prospects for discovery

The above detectors will enhance the sensitivity at energies above 10 PeV to unprecedented levels. Fig. 3.5 [83] compares the sensitivities of the different experiments and the current measurement on neutrino fluxes. Besides the aforementioned upper bound by IceCube [74], there is another upper bound coming from the non-observation of neutrino candidates in the ultra-high energy range by the Pierre Auger Observatory [84]. The existing upper bounds on the flux of UHE neutrinos are larger than the theoretical predictions on the flux of cosmogenic neutrinos by a factor of 5 to two orders of magnitude, depending on the chemical composition of UHE cosmic rays, still uncertain.

The sensitivity reached by this new generation of experiments will be sufficient to probe some of the theoretical models of cosmogenic neutrinos (Fig. 3.5) and source neutrinos (compare Fig. 2.4[64]), meaning that they may finally discover UHE neutrinos in the next decade.

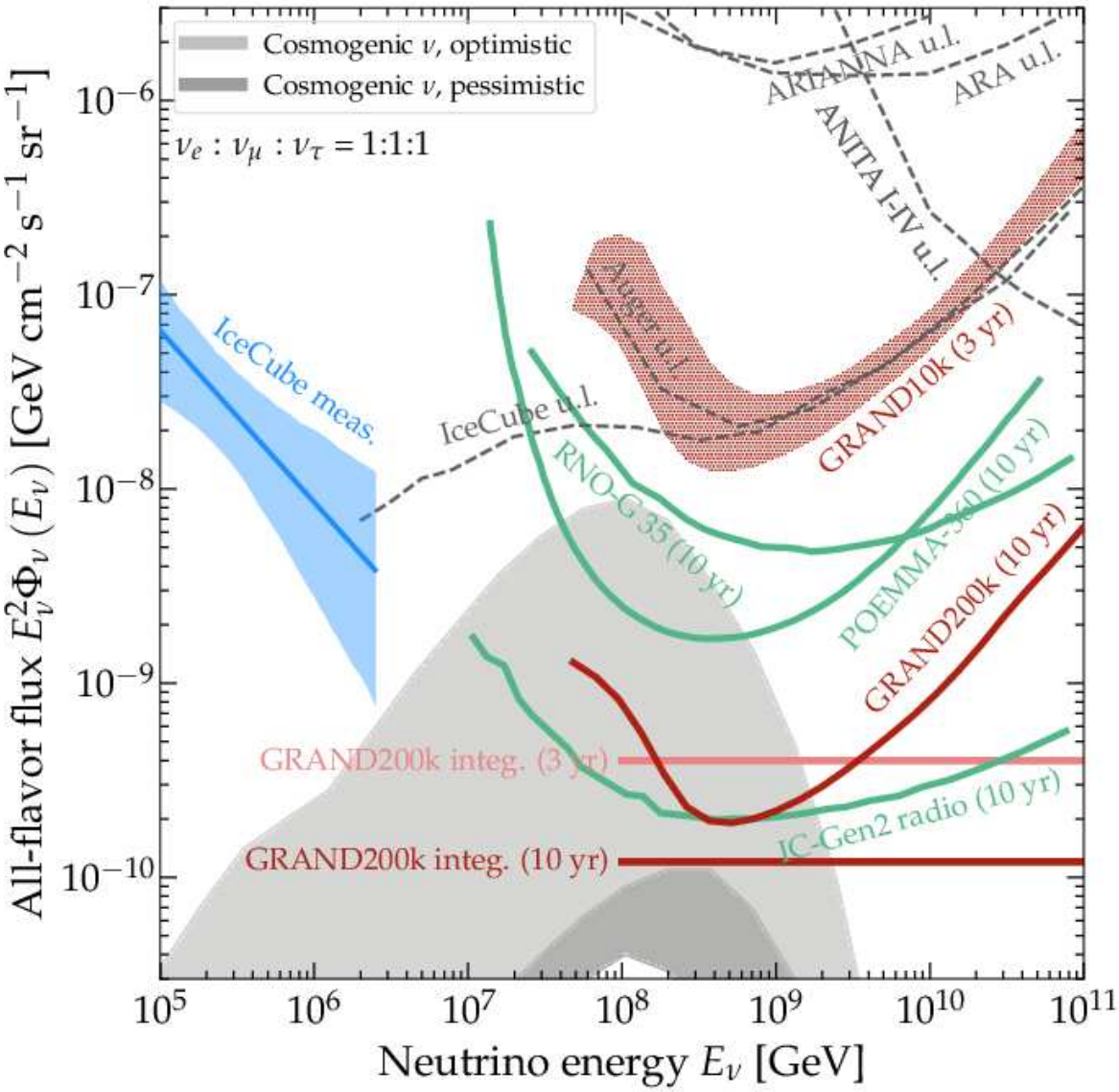

Figure 3.5: **UHE neutrino telescopes: prospects for discovery.** *Figure taken from Ref. [83].*

Chapter 4

Measuring flavor at ultra-high energies: a two-detector approach

The discovery of UHE neutrinos may be within reach in the next decade, thanks to the new generation of dedicated neutrino telescopes. Once discovered, the characterization of their properties would shed light on the primaries UHE cosmic rays, whose origin, production mechanisms and propagation stand among the unsolved mysteries of astroparticle physics. To tackle these questions it will be interesting to measure different observables of UHE neutrinos, such as their distribution in energy and in arrival direction, and their flavor composition, *i.e.*, the proportion of neutrinos of different flavor, ν_e, ν_μ, and ν_τ, in their flux.

In this chapter we elaborate on the flavor of high-energy cosmic neutrinos, reviewing its relation to astrophysics and particle physics, and how it can be measured. Then, we focus on UHE cosmic neutrinos and we present a novel idea to perform a measurement of the flavor composition at ultra-high energy. We explore the sensitivity that can be obtained with this alternative approach, showing the full analysis and presenting the first measurement forecasts of the flavor composition at ultra-high-energy available in the literature [85].

4.1 The flavor composition of cosmic neutrinos

The flavor composition of cosmic neutrinos is a versatile observable, as it encodes information on their astrophysical origin and production mechanism, but also on the fundamental particle physics that governs their propagation and oscillations.

In the following we denote the ratio of the differential flux of $\nu_\alpha + \bar{\nu}_\alpha$, Φ_α, to the all-flavor flux by $f_\alpha \equiv \Phi_\alpha / \sum_\alpha \Phi_\alpha$, with the subscripts S or $\oplus$ to refer to the fraction emitted at source or the one that arrives on Earth, respectively.

The initial flavor composition with which neutrinos are produced depends on the physical process that generated them, and on the properties of the environment in which they are produced. More specifically, the physical mechanisms that are at work in the production of high-energy neutrinos are the decay of charged mesons, mostly pions, and the decay of neutrons, all stemming from the interactions of cosmic rays with hadrons and photons, at their source or during their propagation. The decay chain of charged pions, $\pi^+ \to \mu^+ + \nu_\mu$ followed by $\mu^+ \to \bar{\nu}_\mu + e^+ + \nu_e$ (and their charge-conjugated processes), produces a flavor composition at source $(f_{e,\mathrm{S}}, f_{\mu,\mathrm{S}}, f_{\tau,\mathrm{S}}) \equiv$

$\left(\frac{1}{3}, \frac{2}{3}, 0\right)_{\rm S}$, hereafter called "pion decay"composition. This is the standard expectation.

However, if the neutrinos are produced in regions that host an intense magnetic field, the radiative losses of the intermediate muon due to synchrotron emission can be significant, cooling it down to lower energies before decaying. Therefore, the resulting electron and muon (anti-)neutrinos have low energies, and the flavor composition of the high energy flux moves towards the "muon damped" composition, $(0, 1, 0)_{\rm S}$.

High-energy $\bar{\nu}_e$ are also produced in the β-decay of free neutrons, yielding the "neutron decay" composition, $(1, 0, 0)_{\rm S}$. These high-energy cosmic neutrons can be produced by photo-disintegration of UHE nuclei accelerated in compact sources [86, 87], or by the interactions of accelerated protons with ambient protons $p + p \to n + X$ [88]. Because the difference between the mass of the neutron and the proton it decays into is small, the $\bar{\nu}_e$ they produce are typically of lower energy.

The expected value of $f_{\tau,{\rm S}}$ is 0, since ν_τ come from the decay of charmed mesons, whose production is suppressed [89, 90, 91].

This initial flavor composition oscillates into the one that we observe on Earth, $\boldsymbol{f}_\oplus \equiv (f_{e,\oplus}, f_{\mu,\oplus}, f_{\tau,\oplus})$. Since the distances traveled by high-energy cosmic neutrinos, of Mpc-Gpc, are much larger than the oscillation length, and since the energy resolution of neutrino telescopes is unable to resolve rapid oscillation patterns, the oscillating term in the oscillation probability, Eq. (1.1), is averaged out. Thus, the oscillation probability for $\nu_\alpha \to \nu_\beta$ has the simpler expression

$$P_{\nu_\alpha \to \nu_\beta} = \sum_i |U_{\alpha i}|^2 |U_{\beta i}|^2 \,, \tag{4.1}$$

where U is the lepton mixing matrix. In our work below, we assume the normal neutrino mass ordering (see Chapter 1), and use the best-fit parameters from the NuFIT 5.2 global fit to oscillation data [28] (including Super-Kamiokande atmospheric data). We do not consider in our analysis the uncertainties on the oscillations parameters, since our projections refer to experiments that will be completed in the next decade: we assume that by 2040 the precision of the parameters to have improved to the point where they introduce only a small uncertainty on the predicted flavor composition of high-energy cosmic neutrinos [92].
Fig. 4.1 shows how the three benchmark flavor compositions at source previously discussed are modified by standard neutrino oscillations.

Being able to measure the flavor composition of cosmic neutrinos would be of interest for astrophysics, since it would reveal the dominant mechanism in which these neutrinos are produced, but also for fundamental physics, where it could unveil new physics governing neutrino oscillations. However, as it will be clear in the next section, measuring the flavor composition of cosmic neutrinos is not easy, as there are multiple obstacles keeping us away from pin-pointing with precision its value.

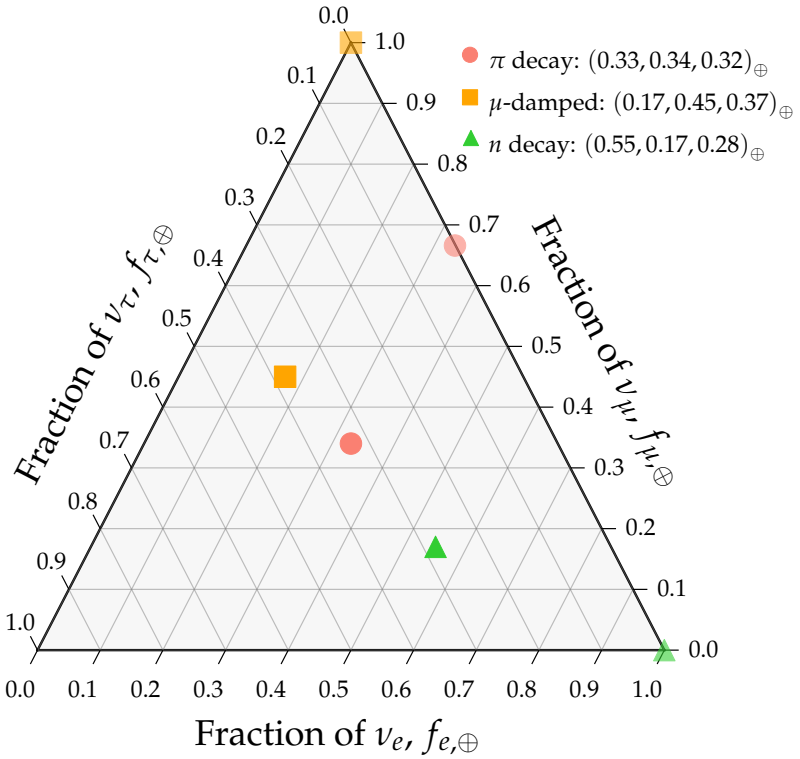

Figure 4.1: **Flavor composition of high-energy cosmic neutrinos.** *The three benchmark flavor compositions are showed at source (light-colored) and at Earth, after neutrino oscillations (dark-colored).*

4.2 Measuring the flavor composition

To infer the flavor of the neutrino that started an event, the detector should be able to discriminate the different flavors based on the experimental signature. This is the case for IceCube, where high-energy neutrinos of different flavors produce different event topologies. IceCube is able to discriminate muon tracks, made primarily by CC interactions of ν_μ, from particle showers, made by all other interactions. The CC interactions of ν_e and ν_τ are poorly distinguished in the detector, as they mostly produce cascades with similar topologies (except for double bang signatures). This limits the flavor-measurement capabilities of IceCube, which can constrain mostly the fraction of $\nu_\mu + \bar{\nu}_\mu$ in the total flux.

Fig. 4.2 [49] shows the results of a previous analysis on the flavor composition of astrophysical neutrinos. With the recent 5 σ observation of tau neutrino signatures [48], new studies will be necessary.

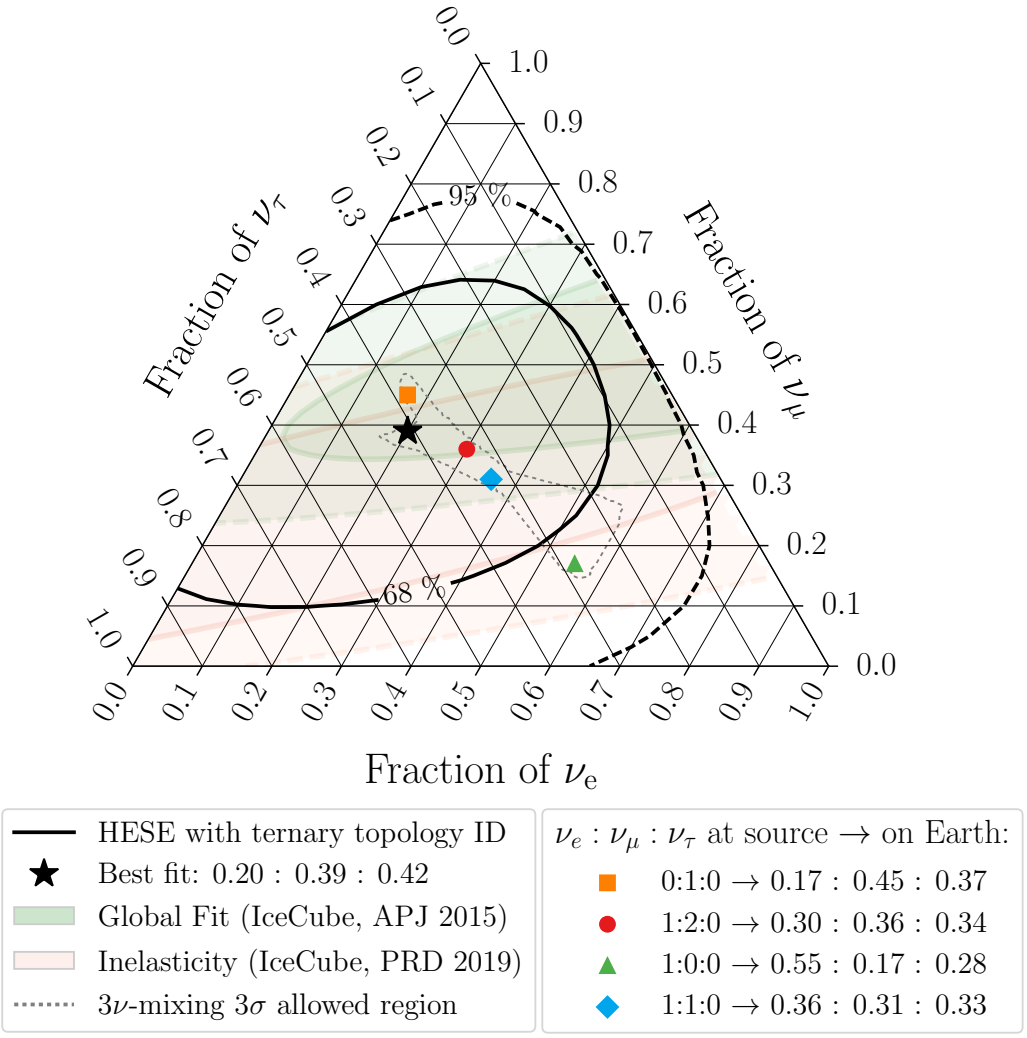

Figure 4.2: **Measured flavor composition of 7.5 years of IceCube HESE events.** *The shaded regions show previously published results [93, 94] without direct sensitivity to the tau neutrino component. Colored markers show the flavor composition at Earth for the benchmark source compositions discussed in this chapter. The dotted region represents the full accessible range of flavor compositions, assuming standard 3-flavor mixing. Figure taken from Ref. [49].*

As we saw in Chapter 3, while IceCube detects cosmic neutrinos with energies in the TeV–PeV, its active volume is not sufficient to detect the low fluxes expected for UHE neutrinos, and we hope to detect them via the radio arrays that will be built in the next decade. In particular, a flavor measurement similar to those performed by IceCube would need the new detectors to discriminate the radio signatures stemming from different interactions.

These UHE neutrino telescopes are still under planning, and research is ongoing to explore the possibility to measure the flavor composition within an individual detector [95, 96, 97]. A recent work [98] showed that it could be possible to measure the UHE neutrino flavor composition in the radio array of IceCube-Gen2. However, the techniques proposed there yield sensitivity to ν_e, on the one hand, and to $\nu_m u + \nu_t au$, on the other. There is no sensitivity to ν_τ by itself.

4.3 Flavor sensitivity with two detectors

We propose a novel idea to measure the flavor composition of UHE neutrinos, that does not rely on the flavor-identification capabilities of an individual detector. We manufacture flavor sensitivity combining the information from two planned detectors: one that detects all neutrino flavors roughly indistinctly—*e.g.*, the planned radio array of IceCube-Gen2—and one that detects predominantly ν_τ—*e.g.*, GRAND. This allows us to measure the fraction of ν_τ in the diffuse UHE flux, even if future detectors will not be able to measure flavor independently. This sensitivity to ν_τ would complement uniquely the flavor measurement of IceCube-Gen2, if that will be possible [98]. The question is whether the sensitivity obtained in this way will be sufficient to give meaningful constraints on the flavor composition. In the following we address this question and present the full sensitivity study for this two-detector measurement.

We perform the analysis combining the events detected in the radio array of IceCube-Gen2, sensitive to all flavors, and in GRAND, which is sensitive mostly to $\nu_\tau + \bar{\nu}_\tau$. Since GRAND is still under planning we perform the analysis on the smallest configuration, GRAND10k, and the intermediate one, GRAND50k.

This section is organized as follows: first, we discuss the simulations of the neutrino events, by showing the modeling of the flux and the characterization of the experiments. Then, we introduce our statistical analysis, showing the steps used to constrain the parameters. Finally, we present the results of our analysis, namely the measurement forecasts of the flavor composition at ultra-high energy, for different benchmark fluxes and experimental configurations.

4.3.1 Neutrino flux

We showed in Fig. 2.4 the landscape of neutrino flux models. To simulate the flavor reconstruction potential of our two-detector method we first need to assume a flux for UHE neutrinos. In this work we will not consider any specific source but parameterize the diffuse flux Φ of UHE $\nu + \bar{\nu}$ of each flavor α with a log-parabola

$$E_\nu^2 \Phi_\alpha = \Phi_0 f_{\alpha,\oplus} \exp\left[-w \log^2\left(\frac{E_\nu}{E_{\rm bump}}\right)\right], \tag{4.2}$$

where E_ν is the neutrino energy measured at Earth, Φ_0 is the normalization of the all-flavor flux, w is the width of the log-parabola, and $E_{\rm bump}$ the energy at which it peaks.

As benchmark, we choose the diffuse flux parameters $\boldsymbol{\theta} \equiv (\Phi_0, w, E_{\rm bump})$ in order to approximate the predicted flux from newborn pulsars [65]. We find good agreement, especially at the highest energies, for $\Phi_0 = 1.5 \cdot 10^{-8}$ GeV cm^{-2} s^{-1} sr^{-1}, $w = 0.25$, and $E_{\rm bump} = 3 \cdot 10^8$ GeV. This flux yields $\mathcal{O}(100)$ all-flavor events in 10 years in IceCube-Gen2, and in the following we will refer to it as the "high" flux. To test the sensitivity that can be obtained with a reduced statistics, we compute events also for a diffuse flux with a normalization Φ_0 ten times smaller, in the following denoted the "low" flux.
In Fig. 4.3 [85] we show the two benchmark fluxes, together with the experimental sensitivities of IceCube-Gen2 and GRAND.

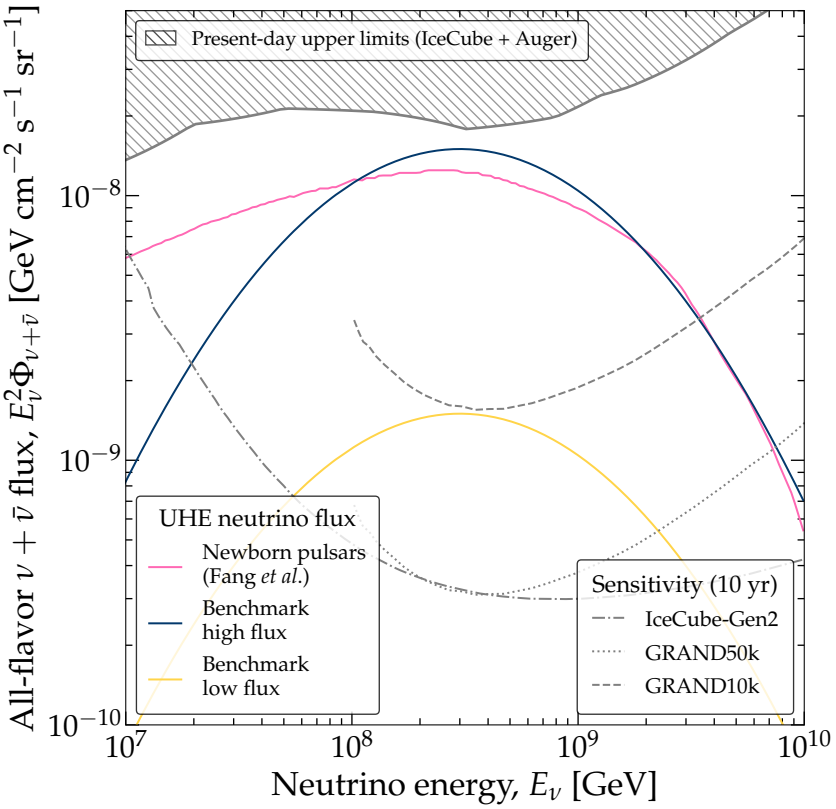

Figure 4.3: **UHE neutrino flux benchmark models used in our analysis.** *The sensitivity of the radio array of IceCube-Gen2 is from Ref. [99]. The sensitivities of GRAND50k and GRAND10k are computed by inverting Eq. (4.4), using the effective areas of GRAND50k and GRAND10. The upper limits are from IceCube [100] and Auger [101]. Figure taken from Ref. [85].*

4.3.2 Detector response

The next step is to model the detection in the two experiments, IceCube-Gen2 and GRAND, and compute the mean expected number of detected events for a given flux. This will provide the mock dataset over which we will perform the statistical analysis to reconstruct the flavor.

The differential event rate for neutrinos of flavor α and energy E_ν in a detector (det) is

$$\frac{dN_\alpha^{\rm det}}{dE_\nu} = \Omega\, T\, \Phi_\alpha\, A_\alpha^{\rm det}\ , \tag{4.3}$$

where Ω is the solid angle of the sky to which the detector is sensitive, T is the detector exposure time, and $A_\alpha^{\rm det}$ is the effective area of the detector for ν_α. We consider an exposure time of 10 years, representative of the design runtimes of the radio array of IceCube-Gen2 and GRAND.

For the radio array of IceCube-Gen2, even though we do not attribute to it flavor-identification capabilities, we compute the contributions of neutrinos of different flavors separately. To this end, we use flavor-specific effective areas, which we build in three steps. First, we infer the flavor-averaged effective area from the reported sensitivity of

IceCube-Gen2 $S(E_\nu)$, from Ref. [99] (see Fig. 4.3), as

$$A_{\rm avg}^{\rm IC\text{-}Gen2} = \frac{2.44 E_\nu}{\Omega\ S(E_\nu)\ T \ln 10}\ , \tag{4.4}$$

where we assume that the sensitivity is defined using the background-free prescription in the Feldman-Cousins approach [102], with 2.44 events at 90% C.L.. Here we require 2.44 events per energy decade, yielding the additional $\ln 10$ in the denominator. In this case, $\Omega = 4\pi$ because the sensitivity is reported as all-sky. Second, we use the flavor-specific effective areas, $A_e^{\rm IC\text{-}Gen2}$, $A_\mu^{\rm IC\text{-}Gen2}$, and $A_\tau^{\rm IC\text{-}Gen2}$, of the `toise` simulation framework [103] (see also Ref. [104]), which provides the simulated effective areas to neutrinos of each flavor for a benchmark in-ice radio-based neutrino telescope; see Fig. 16 in Ref. [103]. From them, we compute the flavor-averaged effective area, $(\sum_\alpha A_\alpha^{\rm IC\text{-}Gen2})/3$. Third, and finally, we equate this to $A_{\rm avg}^{\rm IC\text{-}Gen2}$ from Eq. (4.4) to reweigh the flavor-specific effective areas. Thus, the resulting areas, which we use in our forecasts, reflect both the flavor sensitivity of the detector and its most recent flux-discovery potential. Because we do not ascribe flavor-identification capabilities to the radio array of IceCube-Gen2, we use the event rate summed over all flavors, *i.e.*,

$$\frac{dN^{\rm IC\text{-}Gen2}}{dE_\nu} = \sum_\alpha \frac{dN_\alpha^{\rm IC\text{-}Gen2}}{dE_\nu}\ , \tag{4.5}$$

where the contribution of each flavor is computed using Eq. (4.3) with the flavor-specific effective area.

For GRAND, in order to make our estimates conservative, we do not use the full planned configuration of the experiment, but smaller sizes only, GRAND50k and GRAND10k. To model the detection we start with the effective area of the full-sized array, GRAND200k, reported by the Collaboration in Fig. 25 of Ref. [82]. The effective area is defined for ν_τ only and for detection of neutrinos from 3°–4° around the horizontal direction, including the contribution of a nearby mountain where neutrinos can interact, *i.e.*, $\Omega = 2\pi(\cos 86° - \cos 93°)$, where the angles are zenith angles measured from the South Pole. For GRAND50k and GRAND10k, we divide the GRAND200k effective area by 4 and 20, respectively.

We ignore the potential subdominant contribution of neutrinos of other flavors interacting with the air near the detector [82], since it has not been estimated in detail yet. Thus, for GRAND50k, we use the event rate due to ν_τ only, *i.e.*,

$$\frac{dN^{\rm GRAND50k}}{dE_\nu} = \frac{dN_\tau^{\rm GRAND50k}}{dE_\nu}\ , \tag{4.6}$$

computed using Eq. (4.3) with the effective area of GRAND50k estimated as outlined above, and similarly for GRAND10k.

For each detector, we compute the event rate in the i-th energy bin by integrating the differential event rate over the width of the bin, $\Delta E_{\nu,i}$, *i.e.*,

$$N_i^{\rm det} = \int_{\Delta E_{\nu,i}} \frac{dN^{\rm det}}{dE_\nu} dE_\nu\ . \tag{4.7}$$

We use four energy bins per energy decade, evenly spaced in logarithmic scale, from $5 \cdot 10^6$ to $5 \cdot 10^{10}$ GeV for IceCube-Gen2 and from 10^8 to 10^{11} GeV for GRAND, the energy ranges reported in Refs. [99, 82].

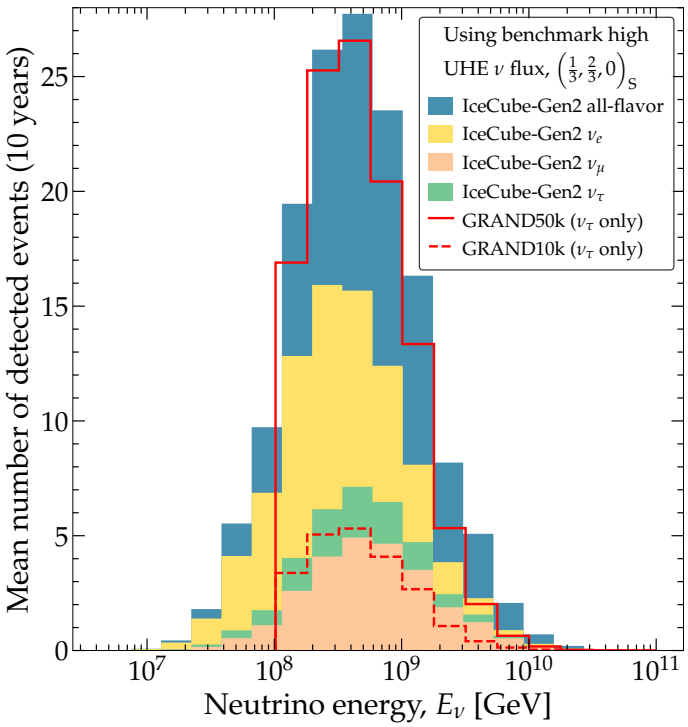

Figure 4.4: **Mean expected number of detected events in the radio array of IceCube-Gen2 and GRAND.** *The event rates are computed assuming the benchmark high UHE neutrino flux and the pion decay composition. For the benchmark low flux, the event rates (not shown) are ten times smaller. Figure taken from Ref. [85].*

Figure 4.4 shows the mean expected energy distributions of events computed assuming our high benchmark UHE neutrino flux. The bin sizes are the same for both detectors, but their positions are slightly different because the energy ranges of IceCube-Gen2 and GRAND that we use are different.

4.3.3 Statistical analysis and results

The last step to reconstruct the flavor of the simulated events is to perform a statistical analysis on the mock dataset, to finally obtain the confidence intervals for the flavor composition at Earth.

In order to do that, we start computing, using the methods discussed so far, the *true* mean expected number of detected events in IceCube-Gen2 and GRAND, $\bar{\mu}_{\text{IC-Gen2}}$, and $\bar{\mu}_{\text{GRAND}}$, *i.e.*, what we assume to be our measured dataset. Then, for *test* fluxes, *i.e.*, for test values of the flux shape parameters $\boldsymbol{\theta} \equiv (\Phi_0, w, E_{\text{bump}})$ and of the flavor composition $\boldsymbol{f}_\oplus \equiv (f_{e,\oplus}, f_{\mu,\oplus}, f_{\tau,\oplus})$ in Eq. (4.2), we compute the mean expected numbers, $\mu_{\text{IC-Gen2}}(\boldsymbol{f}_\oplus, \boldsymbol{\theta})$ and $\mu_{\text{GRAND}}(\boldsymbol{f}_\oplus, \boldsymbol{\theta})$. These computations are performed numerically.

The *true* and *test* event samples are compared in each bin in each experiment via Poisson likelihood functions, which are summed into a total likelihood,

$$\ln \mathcal{L}(\boldsymbol{f}_\oplus, \boldsymbol{\theta}) = \sum_i^{\text{bins}} \left[\bar{\mu}_{i,\text{IC-Gen2}} \ln \mu_{i,\text{IC-Gen2}}(\boldsymbol{f}_\oplus, \boldsymbol{\theta}) - \mu_{i,\text{IC-Gen2}}(\boldsymbol{f}_\oplus, \boldsymbol{\theta})\right] + (\text{IC-Gen2} \to \text{GRAND}) \,. \tag{4.8}$$

This function quantifies the discrepancy between the *true* data, computed with the flux shape parameters of the benchmark fluxes and assuming a specific flavor composition, and the expected data for a set of *test* parameters.

In order to find the confidence intervals on the flavor composition parameters, it is first necessary to consider the effects of our ignorance on the true value of the flux parameters. To this purpose, we build our test statistic by minimizing the likelihood over the flux shape parameters,

$$\Lambda(\boldsymbol{f}_\oplus) = 2\left[\min_{\boldsymbol{\theta}} \ln \mathcal{L}(\boldsymbol{f}_\oplus, \boldsymbol{\theta}) - \ln \bar{\mathcal{L}}\right] \ , \tag{4.9}$$

where $\bar{\mathcal{L}}$ is the global minimum of the Likelihood of Eq. (4.8), *i.e.* the one computed with the *true* event samples $\mu_{i,\text{IC-Gen2}}(\boldsymbol{f}_\oplus, \boldsymbol{\theta}) \to \bar{\mu}_{i,\text{IC-Gen2}}$ and $\mu_{i,\text{GRAND}}(\boldsymbol{f}_\oplus, \boldsymbol{\theta}) \to \bar{\mu}_{i,\text{GRAND}}$.

Wilks' theorem [105] ensures that Λ follows a χ^2 distribution. The test statistic depends explicitly on three parameters, the flavor ratios at Earth $(f_{e,\oplus}, f_{\mu,\oplus}, f_{\tau,\oplus})$, but since we are considering a unitary evolution between the three flavors it holds that $f_{e,\oplus} + f_{\mu,\oplus} + f_{\tau,\oplus} = 1$, and the independent parameters are two. Thus, the probability distribution of the test statistic is a χ^2 with two degrees of freedom, which we choose to be $f_{e,\oplus}$ and $f_{\mu,\oplus}$ (then $f_{\tau,\oplus} \equiv 1 - f_{e,\oplus} - f_{\mu,\oplus}$).

We compute Λ on a grid of $(f_{e,\oplus}, f_{\mu,\oplus})$, numerically marginalizing over the nuisance parameters $\boldsymbol{\theta}$ and setting as initial guess the true parameters. Then, we constrain $f_{e,\oplus}$ and $f_{\mu,\oplus}$ at the 68% and 95% confidence level (C.L.) by demanding $\Lambda = 2.28$ and 6, respectively, and finally obtain the confidence intervals.

In Figs. 4.5 and 4.6 [85] we show the results of our analysis for a true source composition due to pion decay and muon damped, respectively.
The allowed regions of flavor composition at Earth are shown for the two benchmark fluxes and the two configurations of GRAND, GRAND10k and GRAND50k. The allowed regions are roughly aligned with the $f_{\tau,\oplus}$ axis, since this is the predominant flavor fraction extracted from combining IceCube-Gen2 and GRAND. The misalignment comes from IceCube-Gen2 being slightly more sensitive to ν_e than to the other flavors [103] because they are more likely to trigger radio-emitting electromagnetic showers. This is what allows us to disfavor values of $f_{e,\oplus}$ that differ significantly from its true value of about one third, especially those higher, and what causes the different number of all-flavor events between the pion decay and muon-damped compositions.

Assuming a pion decay composition and using GRAND50k, if the flux is high the true flavor composition can be distinguished from the muon-damped one at nearly 95% C.L. and from neutron decay at more than that. If the flux is low, the three benchmarks become indistinguishable at 68% C.L. If only GRAND10k is available, the flavor reconstruction capabilities of the analysis worsens and the true flavor composition can be distinguished at 68% C.L. from the competing models only if the flux is high.

Instead, if the true composition at source is muon-damped, we see that it can be distinguished from the pion decay at more than 68% C.L. if the flux is high, but if the flux is low they become indistinguishable at 68% C.L.. The neutron decay composition can be ruled out at least at 68% C.L. for both benchmark fluxes. Using GRAND10k the statistics is reduced and the sensitivity is lower: the true composition cannot be distinguished from the pion decay one at 68% C.L., even if the flux is high. Moreover, if the flux is low, not even the neutron decay composition can be excluded at 68% C.L..

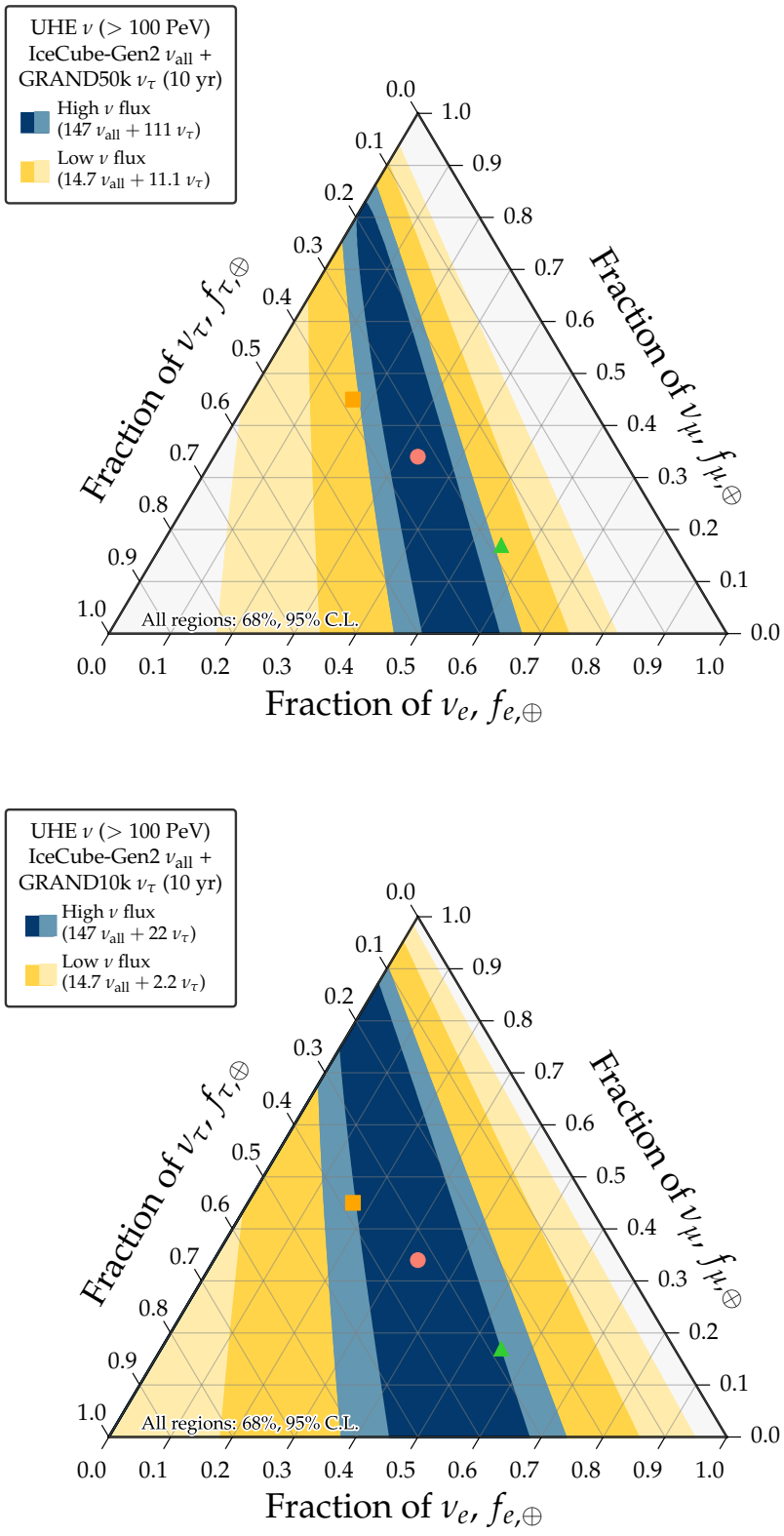

Figure 4.5: **Projected measurement of the flavor composition at Earth of ultra-high-energy neutrinos, for a pion decay true composition.** *The regions are of allowed flavor composition, obtained by combining measurements of neutrinos of all flavors in the radio array of IceCube-Gen2 and of ν_τ in GRAND50k (top) and GRAND10k (bottom). Figures taken from Ref. [85].*

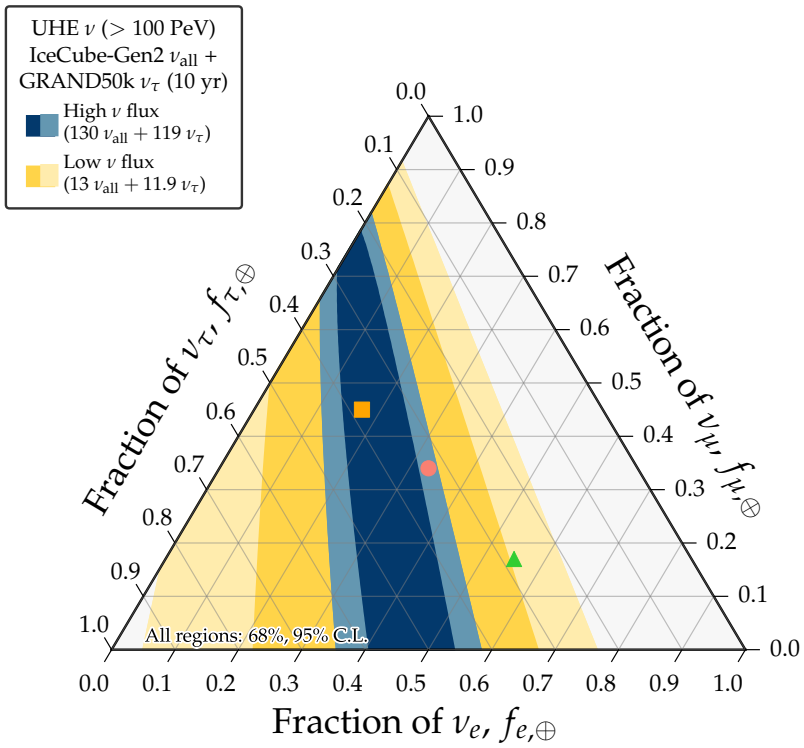

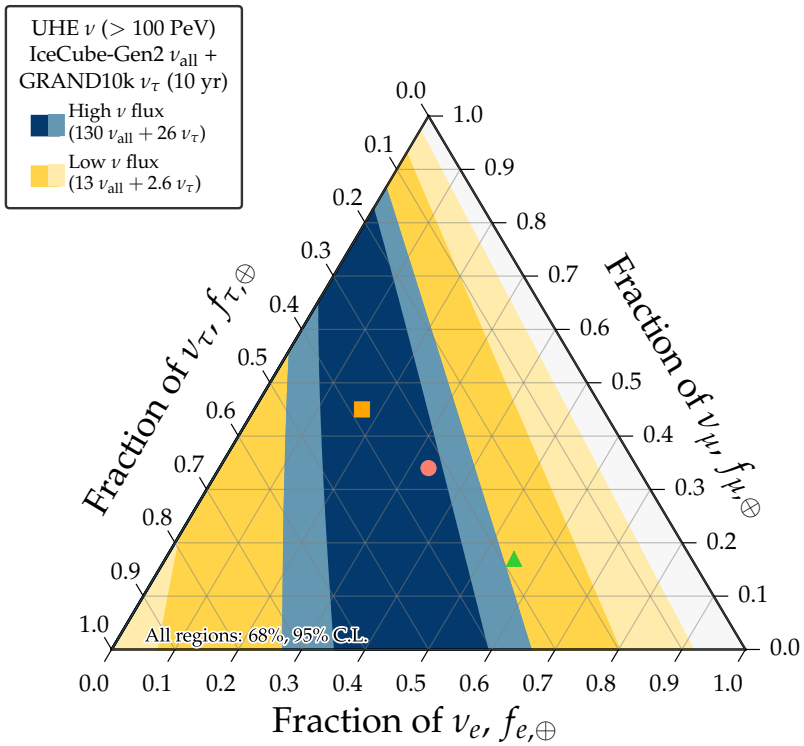

Figure 4.6: **Projected measurement of the flavor composition at Earth of ultra-high-energy neutrinos, for a muon damped true composition.** *Same as Fig. 4.5, but assuming that the true flavor composition is muon-damped. Figures taken from Ref. [85].*

Chapter 5

Applications to astrophysics and particle physics

In the preceding chapter, we introduced a novel idea to measure the flavor composition of neutrinos in the ultra-high energy range, and we showed how our analysis could constrain this observable even under conservative assumptions.
Next, we apply our technique in astrophysics, to infer the flavor composition of UHE neutrinos at their sources, and in fundamental particle physics, to probe non-standard oscillations.

5.1 Flavor content at source

In Section 4.1 we discussed how different neutrino production mechanisms yields different proportions of each flavor. The oscillations of these neutrinos make the flavor composition that we may detect on Earth different from the one at production. If we assume that the physics of oscillations, currently tested with experiments on Earth up to $E_\nu \lesssim 100$ GeV, is still valid at energies of the EeV scale, we can invert the effects of oscillations on the flavor measured on Earth and infer the flavor composition with which neutrinos are produced.

In the following we will perform this analysis on the measurement forecasts that we produced for the flavor composition of the diffuse flux of UHE neutrinos. This will yield confidence intervals for the initial flavor composition, averaged over all the unknown production sites, be they close to astrophysical objects (for source neutrinos) or in the targets that UHECRs can encounter during propagation (for cosmogenic neutrinos).

5.1.1 Analysis and results

We use the techniques first introduced in Ref. [106] (see also Ref. [92]) and adapt the analysis used in Section 4.3.3 to infer the flavor composition at source. Indeed, assuming standard three-flavor oscillations, we have that $f_{\alpha,\oplus} = P_{\alpha\beta} f_{\alpha,\mathrm{S}}$.

We infer the flavor composition at the sources by running the same analysis of Section 4.3.3 and computing the same test statistic as above, but this time as a function of $\boldsymbol{f}_{\alpha,\mathrm{S}} \equiv (f_{e,\mathrm{S}}, f_{\mu,\mathrm{S}}, f_{\tau,\mathrm{S}})$, *i.e.*, $\mathcal{L}(\boldsymbol{f}_\mathrm{S}, \boldsymbol{\theta}) = \mathcal{L}[\boldsymbol{f}_\oplus(\boldsymbol{f}_\mathrm{S}), \boldsymbol{\theta}]$.
Since we assume that there is no UHE ν_τ production, we have that $f_{\mu,\mathrm{S}} \equiv 1 - f_{e,\mathrm{S}}$ and we need to infer only $f_{e,\mathrm{S}}$. This reduces the test statistic to a single degree of freedom,

so we get the confidence intervals on $f_{e,\mathrm{S}}$ by requiring that $\Lambda\left(f_{e,\mathrm{S}}\right)$ is equal to 0.98 (68% C.L.), 3.8 (95% C.L.) and 8.8 (99.7% C.L.).

Figure 5.1 shows the results assuming that the flavor composition at the sources is from pion decay, $f_{e,\mathrm{S}} = 1/3$. We see that using our high benchmark flux, the true value is inferred with enough precision to separate it from the alternative muon-damped and neutron-decay compositions at more than 95% C.L. and 99.7% C.L., respectively. Using our low flux, the separation worsens, but remains significant against neutron decay. Similar conclusions hold when using GRAND10k, but also if we assume a muon damped composition $(0, 1, 0)_{\mathrm{S}}$, as shown in Fig. 5.2.

Distinguishing between the pion-decay and muon-damped flavor composition could constrain the magnetic field intensity in the neutrino sources [107, 108, 109] and, indirectly, their identity. Further, since extragalactic magnetic fields are believed to be weak, inferring a flavor composition compatible with muon-damped could hint at the diffuse UHE neutrino flux being of source rather than cosmogenic origin.

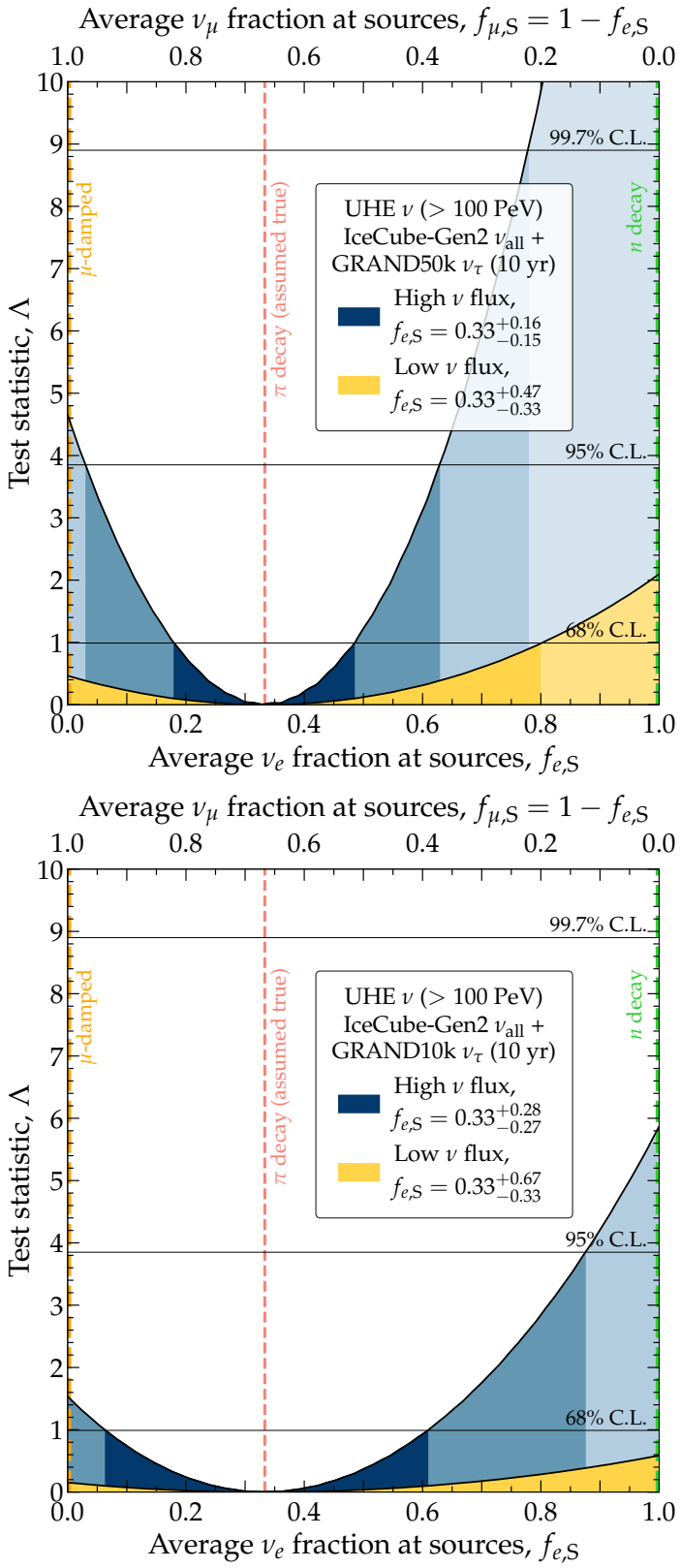

Figure 5.1: **Inferred flavor composition of ultra-high-energy cosmic neutrinos at their sources, assuming neutrino production via pion decay.** *The results are projections obtained from measuring the fraction $f_{\tau,\oplus}$ of ν_τ at Earth by combining the detection by the radio array of IceCube-Gen2 with GRAND50k (top) or GRAND10k (bottom), using methods from Refs. [106, 92]. We assume neutrino production via pion decay, no ν_τ production (i.e., $f_{\tau,S} = 0$), and two benchmark UHE neutrino fluxes, high and low. Figure taken from Ref. [85].*

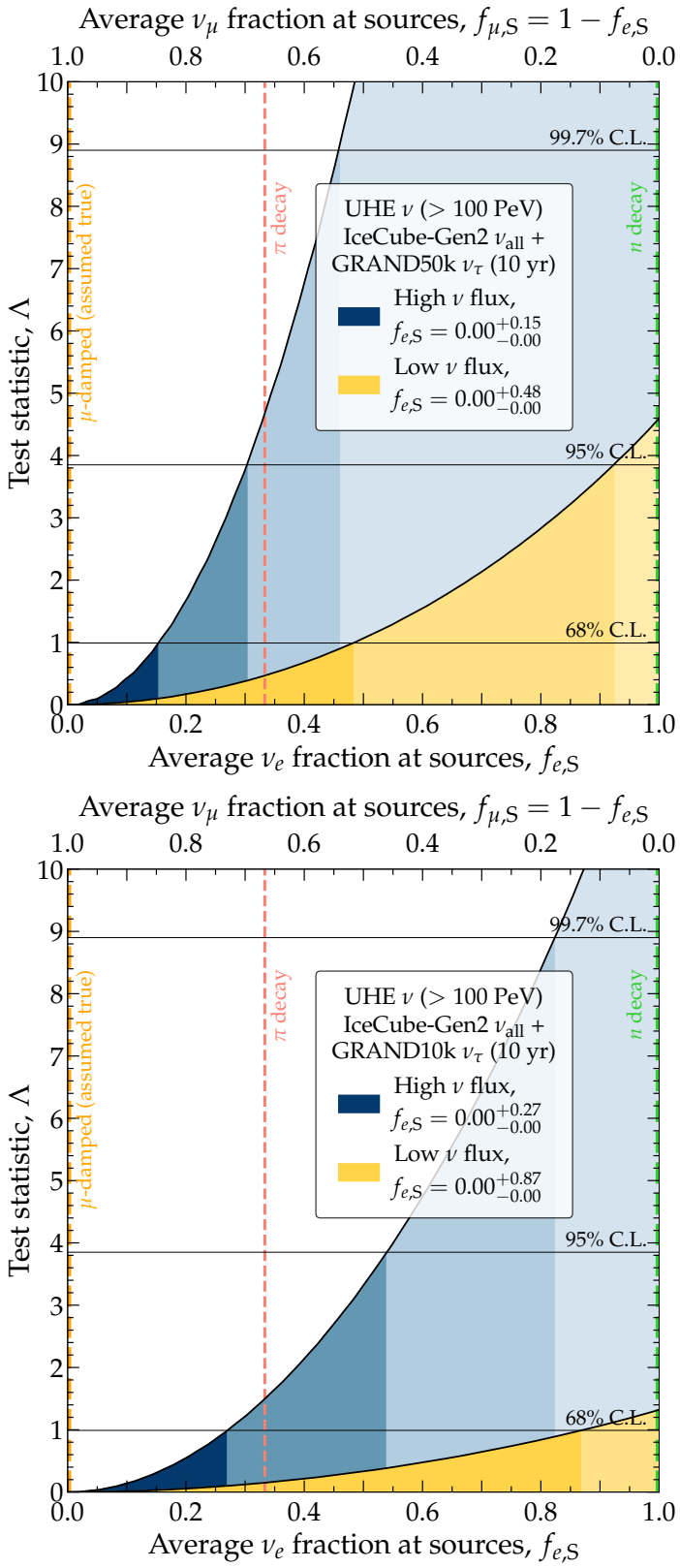

Figure 5.2: **Inferred flavor composition of ultra-high-energy cosmic neutrinos at their sources, assuming a muon-damped composition.** *Same as in Fig. 5.1, but for a muon-damped composition. Figure taken from Ref. [85].*

5.2 Lorentz-invariance violation

A measurement of the flavor composition of neutrinos can also be used to test the standard paradigm of neutrino oscillations. In particular, neutrino oscillations en route to Earth may undergo BSM effects, generating a flavor composition which is different from the expectation from standard oscillations [110, 111, 112, 113, 114, 115, 116]. We focus on a specific BSM feature that can significantly modify the physics of oscillations, Lorentz-invariance violation (LIV).

LIV is possible in some theories of quantum-gravity [117, 118], where Lorentz symmetry can be broken above the Planck mass scale $E \sim M_{\rm pl} = 1.2 \times 10^{19}\,\text{GeV}$. We adopt the LIV treatment from the Standard Model Extension [119, 120, 121, 122], an effective field theory that couples neutrinos to spacetime features. Under LIV, neutrinos are affected by a series of new CPT-odd and CPT-even operators, $\mathring{a}^{(d)}$ and $\mathring{c}^{(d)}$ of dimension d, each a 3×3 matrix in the flavor basis, with units GeV^{4-d}. They modify neutrino mixing via the Hamiltonian $H = H_{\rm std} + H_{\rm LIV}$, where $H_{\rm std} = M^2/(2E_\nu)$ is the standard term that drives oscillations due to the difference in neutrino masses, with $M^2 \equiv (m_1^2, m_2^2, m_3^2)$, and

$$H_{\rm LIV} = \mathring{a}^{(3)} - E_\nu \cdot \mathring{c}^{(4)} + E_\nu^2 \cdot \mathring{a}^{(5)} - E_\nu^3 \cdot \mathring{c}^{(6)} + \dots \,. \tag{5.1}$$

is the contribution from LIV. In this approach, LIV can manifest itself at low energies, but the operators responsible for its observable effects are suppressed by powers of $M_{\rm pl}$.

Eq. (5.1) shows that the intensity of these effects increases with the energy of the neutrino. This makes high-energy and ultra-high-energy cosmic neutrinos excellent probes of deviations from Lorentz symmetry. This is not only because LIV gives rise to energy-dependent features, that can be tested at higher precision with increasing energy, but also because these neutrinos traverse cosmological distances from their production site to Earth, so even small deviations from standard expectations could pile-up, giving rise to observable effects.

So far, there is no evidence for LIV [121], but the strongest limits on it for neutrinos come from measurements of the flavor composition of the IceCube TeV–PeV astrophysical neutrinos [123]. Because the intensity of LIV is expected to grow with neutrino energy—possibly much faster than linearly—using UHE neutrinos promises vast improvement in the discovery or in the limits that can be set on these effects.

5.2.1 Effects of LIV on the diffuse flux of UHE neutrinos

We use our measurement forecasts of the UHE neutrino flavor composition to probe the effects of LIV and set upper limits on the couplings $\mathring{a}^{(d)}$ and $\mathring{c}^{(d)}$, for various operator dimensions.

To consider the effects of LIV on oscillations, we compute the average flavor-transition probability as in Eq. (4.1), but using instead of the PMNS matrix U the energy-dependent matrix that diagonalizes the full Hamiltonian, $\mathcal{U}(E_\nu, \mathring{a}^{(d)}_{\alpha\beta}, \mathring{c}^{(d)}_{\alpha\beta})$. This matrix is equal to the PMNS matrix in the absence of LIV, but it can be different from it, depending on the energy scale and the size of the couplings. We compute it numerically. The expansion of the Universe dampens the energy of the neutrinos, such that the neutrinos that we observe on Earth with energy E_ν from a source located at

at redshift z, were produced with energy $E_\nu(1+z)$. Considering that, the fraction of ν_α detected at Earth is related to the flavor composition at source as

$$f_{\alpha,\oplus}(E_\nu, z) = \sum_{\beta,i} |\mathcal{U}_{\beta i}\,[E_\nu(1+z)]|^2 |\mathcal{U}_{\alpha i}(E_\nu)|^2 f_{\beta,\mathrm{S}} \equiv P_{\nu_\beta\to\nu_\alpha}(E_\nu, z, \mathring{a}^{(d)}_{\kappa\lambda}, \mathring{c}^{(d)}_{\kappa\lambda}) f_{\beta,\mathrm{S}}\ . \quad (5.2)$$

We calculate the flux of UHE neutrinos of different flavors at Earth assuming that the diffuse neutrino flux is due to a population of identical, nondescript astrophysical sources distributed in redshift, each injecting the same neutrino spectrum, ϕ_α. We assume for the sources the same shape that was used for our benchmark diffuse fluxes at Earth,

$$E_\nu^2 \phi_\alpha = \Phi_0 f_{\alpha,\mathrm{S}} \exp\left[-w \log^2\left(\frac{E_\nu}{E_{\mathrm{bump}}}\right)\right]\ . \quad (5.3)$$

The differential diffuse flux of ν_α at Earth, under LIV with coefficients $\mathring{a}^{(d)}_{\kappa\lambda}$ and $\mathring{c}^{(d)}_{\kappa\lambda}$ $(\kappa, \lambda = e, \mu, \tau)$ is computed as

$$\Phi_\alpha(E_\nu, \mathcal{N}, \boldsymbol{\theta}, \boldsymbol{f}_{\mathrm{S}}, \mathring{a}^{(d)}_{\kappa\lambda}, \mathring{c}^{(d)}_{\kappa\lambda}) = \int \frac{dz}{H(z)} \mathcal{N} \rho_{\mathrm{src}}(z) \sum_\beta \phi_\beta[E_\nu(1+z), \boldsymbol{\theta}, \boldsymbol{f}_{\mathrm{S}}] P_{\nu_\beta\to\nu_\alpha}(E, z, \mathring{a}^{(d)}_{\kappa\lambda}, \mathring{c}^{(d)}_{\kappa\lambda})\ . \quad (5.4)$$

In this expression, $\boldsymbol{\theta} \equiv (\Phi_0, w, E_{\mathrm{bump}})$ are the shape parameters of the flux emitted by each source, $\boldsymbol{f}_{\mathrm{S}} \equiv (f_{e,\mathrm{S}}, f_{\mu,\mathrm{S}}, f_{\tau,\mathrm{S}})$ are the flavor fractions at the sources, $H(z) \equiv H_0[\Omega_\Lambda + \Omega_m(1+z)^3]^{1/2}$ is the Hubble parameter, $\Omega_\Lambda = 0.68$ and $\Omega_m = 0.32$ are, respectively, the adimensional energy densities of vacuum and matter [124]. The flux at the source is evaluated at larger energy to account for the cosmological expansion.

We assume that the number density of the sources, ρ_{src}, follows the star-formation rate, parameterized as in Ref. [125], *i.e.*,

$$\rho_{\mathrm{src}}(z) = \frac{(a+bz)h}{[1+(z/c)^d]}\ , \quad (5.5)$$

where $a = 0.017$, $b = 0.13$, $h = 0.7$, $c = 3.3$, and $d = 5.3$, for the modified Salpeter initial mass function [126]. This places most of the sources at $z \approx 2$, a few Gpc away; sources at higher redshifts are rarer and contribute little to the diffuse flux. To simplify the notation we define the overall multiplicative factor $\Phi_0 \mathcal{N} \equiv \mathcal{K}$, and the parameters relative to the all-flavor flux $\boldsymbol{\pi} \equiv (\mathcal{K}, w, E_{\mathrm{bump}})$.

We fix the parameters $\boldsymbol{\pi}$ by demanding that the all-flavor flux, $\sum_\alpha \Phi_\alpha$, approximates the high benchmark flux of Fig. 4.3. This gives $\mathcal{K} = 5 \cdot 10^{-25}$ GeV cm^{-2} s^{-1} sr^{-1}, $w = 0.18$, and $E_{\mathrm{bump}} = 5 \cdot 10^8$ GeV. To reproduce our low benchmark flux we use a normalization constant, $\mathcal{K}$, ten times smaller.

In our notation, $\mathring{a}^{(d)}_{\kappa\lambda}$ and $\mathring{c}^{(d)}_{\kappa\lambda}$ are a basis of complex hermitian matrices that couple only the flavors κ and λ. In general, the flavor composition of astrophysical neutrinos may be modified by a superposition of these operators. If the operators have different dimensions, the different scaling will make the overlap effective only in a reduced energy window, and we assume that this is not the case. However, if the dimensions of the operators are the same, multiple more operators can contribute. Here we want to show the potential of UHE neutrinos for this kind of studies: to simplify the analysis, we turn on a single LIV coefficient at a time when computing the flux, and consider only its real part. In the future, if the statistics will allow it, it could be possible to extend this analysis including multiple operators, with their real and imaginary parts.

5.2.2 Statistical analysis and results

Our goal is to constrain the value of the LIV coefficients. The treatment is analogous to the one used so far: we model the experiments as in Section 4.3.2, compute the distribution of the events detected by each experiment, with and without LIV, and perform a statistical analysis similar to the one of Section 4.3.3, properly modified in order to get the upper bounds on the coefficients.

As before, only two flavor fractions are independent, but since we assume no ν_τ production at source, this number reduces to one; we choose the free parameter to be $f_{e,\mathrm{S}}$, and assume that neutrinos are produced via pion decay, *i.e.*, $f_{e,\mathrm{S}} = \frac{1}{3}$. Again, we perform the analysis for the two benchmark fluxes and the two GRAND configurations.

Since, by combining the radio array of IceCube-Gen2 and GRAND, we are mostly sensitive to the ν_τ fraction, and since from pion decay most of the emitted flux is in ν_μ, we have higher sensitivity to coefficients that inhibit $\nu_\mu \to \nu_\tau$ oscillations, *i.e.*, $\mathring{a}^{(d)}_{e\mu}$, $\mathring{a}^{(d)}_{\tau\tau}$, $\mathring{a}^{(d)}_{e\tau}$, and $\mathring{a}^{(d)}_{\mu\mu}$, and equivalently for $\mathring{c}^{(d)}_{\alpha\beta}$.

Figure 5.3 illustrates the effect of a pure-$\tau\tau$ LIV operator, $[(H_{\mathrm{LIV}})_{\tau\tau}]$, with varying strength relative to standard oscillations, $[(H_{\mathrm{std}})_{\tau\tau}]$, on our three flavor-composition benchmarks. Under weak LIV, we recover standard oscillations. Under dominant LIV, ν_τ mixing is suppressed, until it totally decouples and only $\nu_e \longleftrightarrow \nu_\mu$ is possible. In-between, interference between the standard and LIV contributions creates the wiggles seen in Fig. 5.3. It is clear that when the LIV contribution is dominant the flavor content changes significantly, and that the flavor sensitivity discussed in Chapter 4 is sufficient to probe these deviations from the standard oscillations.

In the notation of Section 4.3.3, the *true* mean number of events, in each detector, $\bar{\mu}_{\text{IC-Gen2}}$, and $\bar{\mu}_{\text{GRAND}}$, is computed assuming $f_{e,\mathrm{S}} = \frac{1}{3}$, fixing the parameters $\boldsymbol{\pi}$ to match the benchmark fluxes of Fig. 4.3 and using the effective areas of the experiment as in Section 4.3.2. Then, for a set of test parameters $(\boldsymbol{\pi}, f_{e,\mathrm{S}}, \mathring{a}^{(d)}_{\kappa\lambda}, \mathring{c}^{(d)}_{\kappa\lambda})$ we compute the corresponding number of events and we build a binned Poissonian Likelihood as in Eq. (4.8). This time, to define our test statistic, we marginalize over the four nuisance parameters $(\boldsymbol{\pi}, f_{e,\mathrm{S}})$. Again, the minimization is performed numerically. To compute the upper limit on the coefficients $\mathring{a}^{(d)}$ and $\mathring{c}^{(d)}$, we follow [127] and set the upper limit at 90% C.L. for $\Lambda = 1.66$.

Figure 5.4 shows our resulting limits for operators of dimension 3–8. Even in the most pessimistic scenario—low neutrino flux and using GRAND10k—all of our projected limits are better than the present ones [123] by orders of magnitude, since H_{LIV} grows with energy. The relative improvement grows with operator dimension, as the energy dependence grows increasingly faster than linearly [Eq. (5.1)]. This is particularly dramatic for dimension-4 and -5 operators, where our limits reach into the quantum gravity-motivated region, unlike existing limits.

Finally, we show analogous results for the operators for which we obtained at least a bound, *i.e.*, those mixing $\nu_\mu - \nu_\mu$ (Fig. 5.5), $\nu_e - \nu_\mu$ (Fig. 5.6) and $\nu_e - \nu_\tau$ (Fig. 5.7). We show results assuming that the flavor composition at the sources is from pion decay. In all cases, our projected limits from UHE neutrinos improve on existing limits. However, for $\mathring{a}^{(d)}_{e\tau}$ and $\mathring{c}^{(d)}_{e\tau}$, limits are achievable only under the most optimistic scenario, using GRAND50k and our benchmark high neutrino flux. This is because the LIV couplings affect directly only ν_e and ν_τ, which make up the smallest contributions to the flux generated by pion decay.

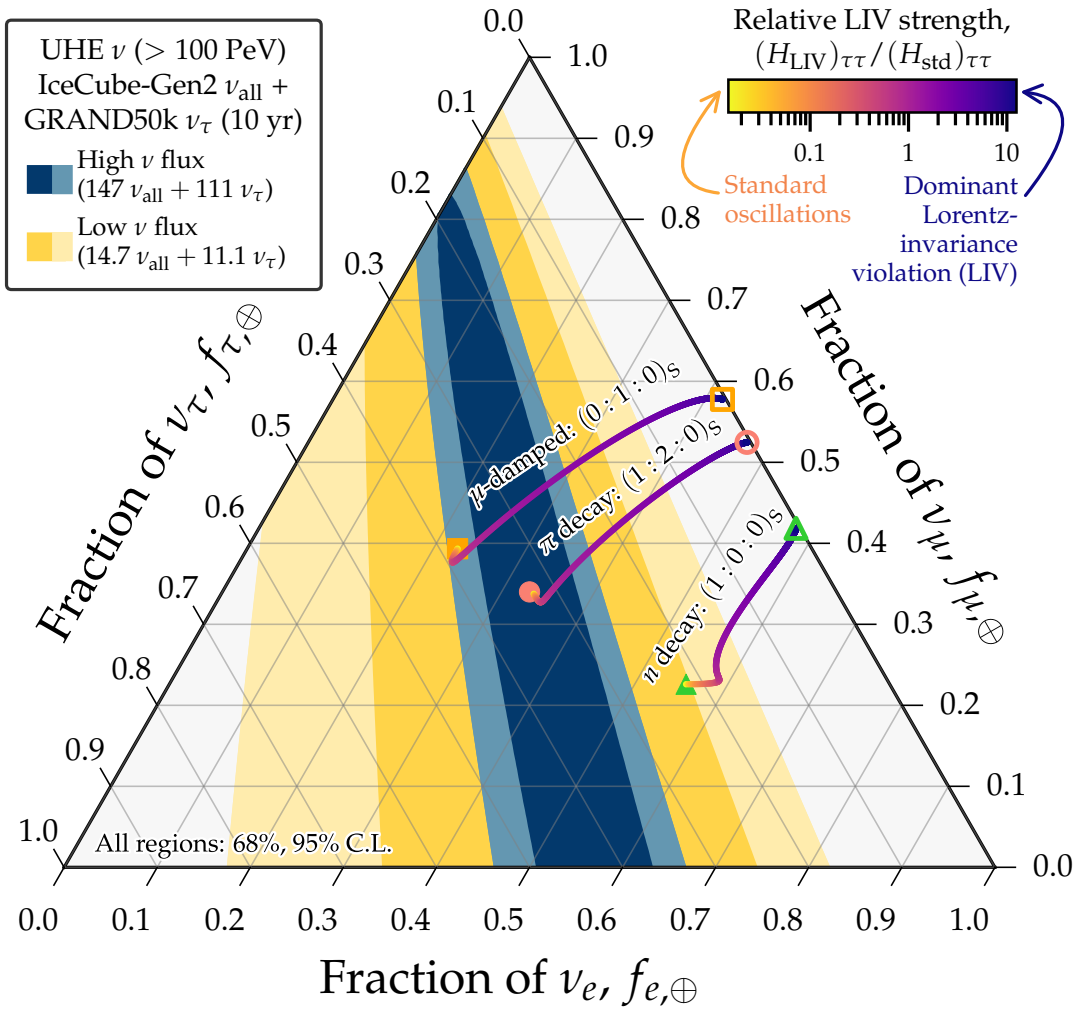

Figure 5.3: **Projected measurement of the flavor composition of ultra-high-energy neutrinos.** *The regions are of allowed flavor composition, obtained with the methods of Chapter 4. Overlaid is the flavor composition at the Earth under standard oscillations and in the presence of Lorentz-invariance violation (LIV) of varying strength, for three benchmarks of the flavor composition at the neutrino sources. Figure taken from Ref. [85].*

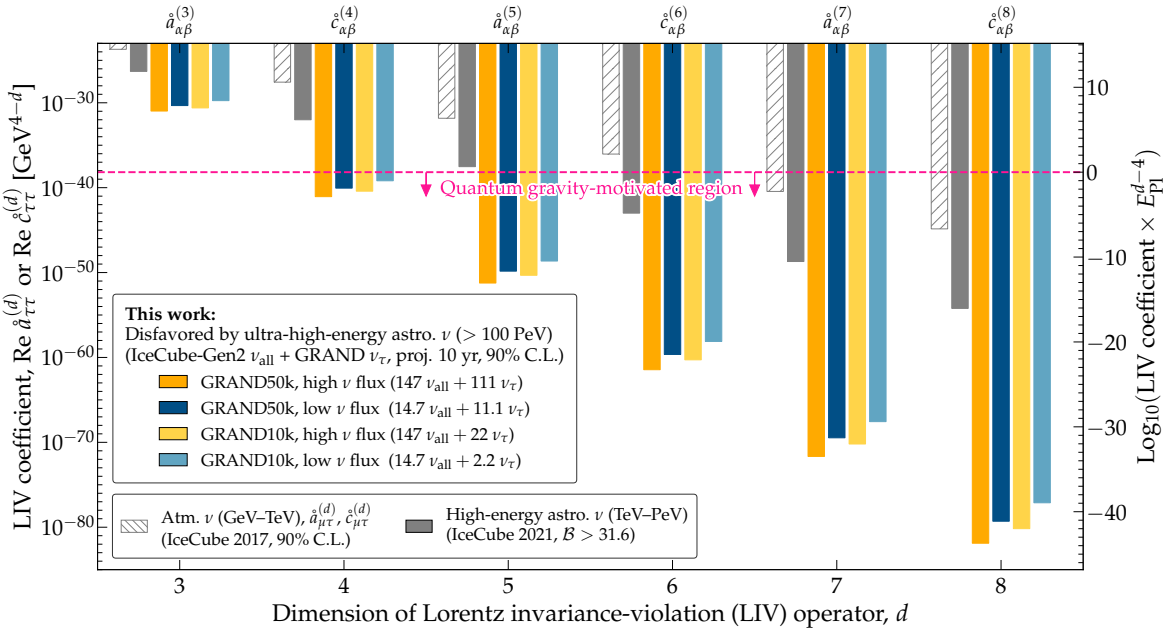

Figure 5.4: **Projected limits on Lorentz-invariance violation (LIV) from ultra-high-energy neutrinos.** *Our limits come from combining the detection of neutrinos of all flavors by the radio array of IceCube-Gen2 and of ν_τ by GRAND. Limits are on the isotropic LIV coefficients $\mathring{a}^{(d)}_{\tau\tau}$ and $\mathring{c}^{(d)}_{\tau\tau}$ of the Standard Model Extension, which are CPT-odd and CPT-even, respectively. Existing limits come from IceCube observations of atmospheric neutrinos [128] (on $\mathring{a}^{(d)}_{\mu\tau}$ and $\mathring{c}^{(d)}_{\mu\tau}$ instead) and TeV–PeV astrophysical neutrinos [123]. For the latter and our projections, we show limits assuming the canonical flavor composition at the sources, $\left(\frac{1}{3}, \frac{2}{3}, 0\right)_\mathrm{S}$. Our limits are profiled over the flavor composition at the sources, and the size and shape of the neutrino spectrum. Figure taken from Ref. [85].*

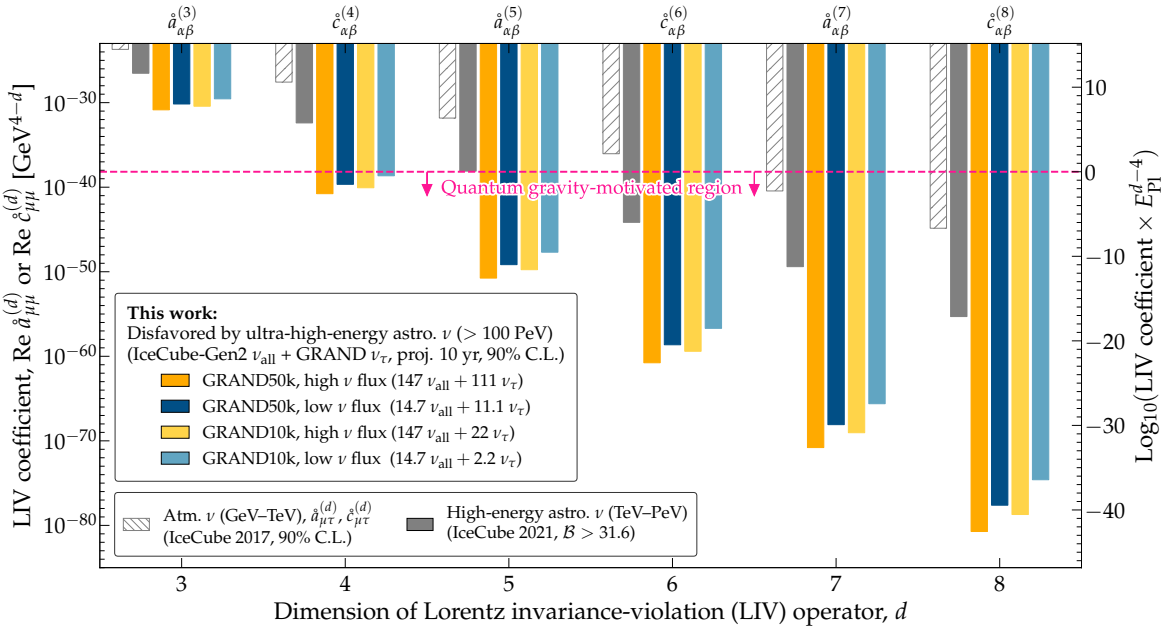

Figure 5.5: **Projected limits on LIV coefficients $\mathring{a}^{(d)}_{\mu\mu}$ and $\mathring{c}^{(d)}_{\mu\mu}$ from UHE neutrinos.** *Figure taken from Ref. [85].*

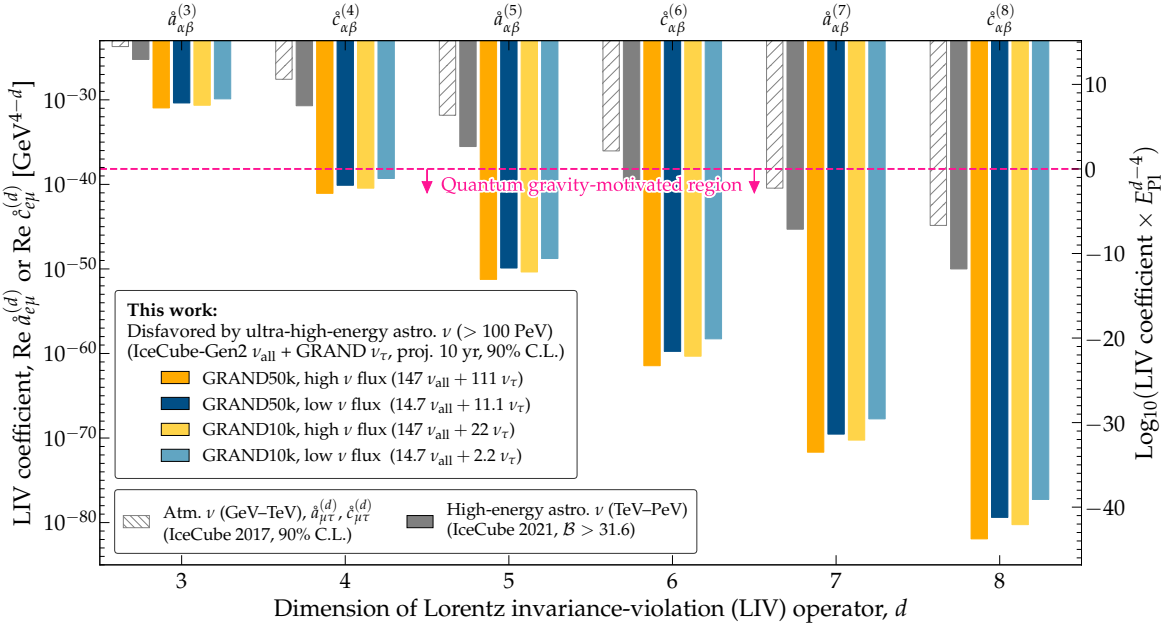

Figure 5.6: **Projected limits on LIV coefficients $\mathring{a}^{(d)}_{e\mu}$ and $\mathring{c}^{(d)}_{e\mu}$ from UHE neutrinos.** *Figure taken from Ref. [85].*

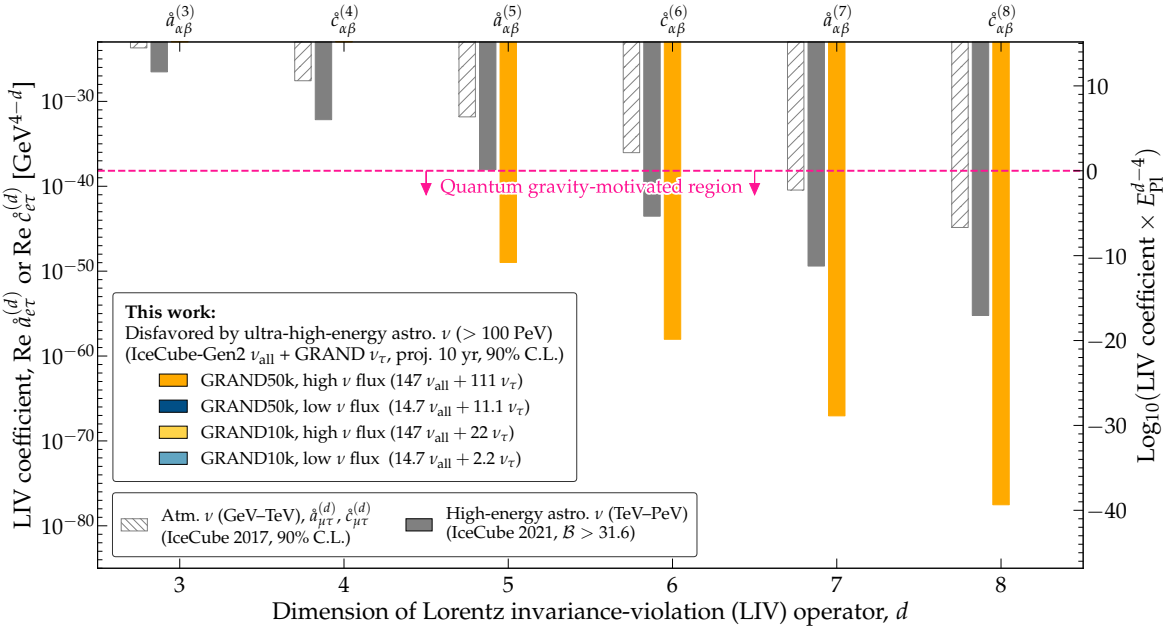

Figure 5.7: **Projected limits on LIV coefficients $\mathring{a}^{(d)}_{e\tau}$ and $\mathring{c}^{(d)}_{e\tau}$ from UHE neutrinos.** *Limits are only achievable in the most optimistic scenario, using GRAND50k and our benchmark high UHE neutrino flux. Figure taken from Ref. [85].*

Chapter 6

Conclusions and outlook

Neutrinos with energies larger than 100 PeV may be discovered in the next decade, opening new frontiers in astrophysics and particle physics. In this work we investigated the possibility to measure the flavor content of the flux of these ultra-high-energy neutrinos. Since it is not clear whether new detectors will have flavor-identification capabilities, we proposed a novel idea to perform this measurement. Flavor sensitivity is manufactured combining the information from two detectors, one sensitive to all flavors–the radio array of IceCube-Gen2–and one sensitive mostly to one flavor–in this work, GRAND, which is sensitive mostly to events initiated by ν_τ. This different approach allows, in principle, to measure the fraction of ν_τ in the all-flavor flux. However, a quantitative analysis was needed, as the intensity and the shape of the flux of UHE neutrinos are largely uncertain and the results of this measurement can depend heavily on them.

In Chapter 4 we performed the analysis for two benchmark fluxes, representative of the breadth of theoretical models, and for the two smallest configurations of GRAND, GRAND10k and GRAND50k. Our work proved that this two-detector approach can constrain the fraction of ν_τ even under conservative assumptions, with 10-20 events detected in 10 years.

This flavor sensitivity, even if limited, can encode a lot of information. In Chapter 5 we used our measurement forecasts to show the physical insights that can be obtained with the flavor of UHE neutrinos. Inverting the effects of oscillations we showed that it could identify the dominant production mechanism of UHE neutrinos, distinguishing between benchmark expectations at 95% C.L. or more and improving our knowledge of the astrophysical environments in which are generated. Then, for fundamental physics, this flavor measurement could lead to vast improvement in the constraints on Lorentz-invariance violation, emblematic of the power to test other new physics that could manifest itself at the highest energies, such as secret neutrino interactions and active-sterile neutrino mixing.

Our methods can be applied to other planned detectors, like RNO-G [76], sensitive to all flavors, and POEMMA [129], sensitive to ν_τ. A recent work [98] showed that in-ice radio-based UHE neutrino telescopes may measure the ν_e and $\nu_\mu + \nu_\tau$ fractions. Our methods would break the degeneracy between ν_μ and ν_τ, providing access to the full flavor composition to tap into its inherent physics potential.

Bibliography

[1] W. Pauli. "Dear radioactive ladies and gentlemen". In: *Phys. Today* 31N9 (1978), p. 27.

[2] J. Chadwick. "Possible Existence of a Neutron". In: *Nature* 129 (1932), p. 312. DOI: 10.1038/129312a0.

[3] Enrico Fermi. "Tentativo di una Teoria Dei Raggi β". In: *Il Nuovo Cimento (1924-1942)* 11 (1934), pp. 1–19. URL: https://api.semanticscholar.org/CorpusID:123342095.

[4] F. Reines and C. L. Cowan. "Detection of the Free Neutrino". In: *Phys. Rev.* 92 (3 Nov. 1953), pp. 830–831. DOI: 10.1103/PhysRev.92.830. URL: https://link.aps.org/doi/10.1103/PhysRev.92.830.

[5] C. L. Cowan et al. "Detection of the Free Neutrino: a Confirmation". In: *Science* 124.3212 (1956), pp. 103–104. DOI: 10.1126/science.124.3212.103. eprint: https://www.science.org/doi/pdf/10.1126/science.124.3212.103. URL: https://www.science.org/doi/abs/10.1126/science.124.3212.103.

[6] John N. Bahcall. "Solar models: An historical overview". In: *Nuclear Physics B - Proceedings Supplements* 118 (Apr. 2003), pp. 77–86. ISSN: 0920-5632. DOI: 10.1016/s0920-5632(03)01306-9. URL: http://dx.doi.org/10.1016/S0920-5632(03)01306-9.

[7] John N. Bahcall. "Solar Neutrinos. I. Theoretical". In: *Phys. Rev. Lett.* 12 (11 Mar. 1964), pp. 300–302. DOI: 10.1103/PhysRevLett.12.300. URL: https://link.aps.org/doi/10.1103/PhysRevLett.12.300.

[8] Raymond Davis. "Solar Neutrinos. II. Experimental". In: *Phys. Rev. Lett.* 12 (11 Mar. 1964), pp. 303–305. DOI: 10.1103/PhysRevLett.12.303. URL: https://link.aps.org/doi/10.1103/PhysRevLett.12.303.

[9] V. A. Kuzmin. "Detection of solar neutrinos by means of the 71Ga(nu, e-)71Ge reaction". In: *Zh. Eksp. Teor. Fiz.* 49 (1965), pp. 1532–1534.

[10] J.N. Abdurashitov et al. "Results from SAGE". In: *Nuclear Physics B - Proceedings Supplements* 48.1 (1996). Proceedings of the Fourth International Workshop on Theoretical and Phenomenological Aspects of Underground Physics, pp. 299–303. ISSN: 0920-5632. DOI: https://doi.org/10.1016/0920-5632(96)00264-2. URL: https://www.sciencedirect.com/science/article/pii/0920563296002642.

[11] W. Hampel et al. "GALLEX solar neutrino observations: results for GALLEX IV". In: *Physics Letters B* 447.1 (1999), pp. 127–133. ISSN: 0370-2693. DOI: https://doi.org/10.1016/S0370-2693(98)01579-2. URL: https://www.sciencedirect.com/science/article/pii/S0370269398015792.

[12] G. Danby et al. "Observation of High-Energy Neutrino Reactions and the Existence of Two Kinds of Neutrinos". In: *Phys. Rev. Lett.* 9 (1 July 1962), pp. 36–44. DOI: 10.1103/PhysRevLett.9.36. URL: https://link.aps.org/doi/10.1103/PhysRevLett.9.36.

[13] M. L. Perl et al. "Evidence for Anomalous Lepton Production in $e^+ - e^-$ Annihilation". In: *Phys. Rev. Lett.* 35 (22 Dec. 1975), pp. 1489–1492. DOI: 10.1103/PhysRevLett.35.1489. URL: https://link.aps.org/doi/10.1103/PhysRevLett.35.1489.

[14] K. Kodama et al. "Observation of tau neutrino interactions". In: *Physics Letters B* 504.3 (Apr. 2001), pp. 218–224. ISSN: 0370-2693. DOI: 10.1016/s0370-2693(01)00307-0. URL: http://dx.doi.org/10.1016/S0370-2693(01)00307-0.

[15] Steven Weinberg. "A Model of Leptons". In: *Phys. Rev. Lett.* 19 (21 Nov. 1967), pp. 1264–1266. DOI: 10.1103/PhysRevLett.19.1264. URL: https://link.aps.org/doi/10.1103/PhysRevLett.19.1264.

[16] Takaaki Kajita. "Atmospheric neutrino results from Super-Kamiokande and Kamiokande — Evidence for oscillations". In: *Nuclear Physics B - Proceedings Supplements* 77.1 (1999), pp. 123–132. ISSN: 0920-5632. DOI: https://doi.org/10.1016/S0920-5632(99)00407-7. URL: https://www.sciencedirect.com/science/article/pii/S0920563299004077.

[17] Pawel Przewlocki. "A study of neutrino interactions constituting the background to electron neutrino appearance in T2K experiment". In: ().

[18] Y. Fukuda et al. "Measurements of the Solar Neutrino Flux from Super-Kamiokande's First 300 Days". In: *Phys. Rev. Lett.* 81 (6 Aug. 1998), pp. 1158–1162. DOI: 10.1103/PhysRevLett.81.1158. URL: https://link.aps.org/doi/10.1103/PhysRevLett.81.1158.

[19] Q. R. Ahmad et al. "Direct evidence for neutrino flavor transformation from neutral current interactions in the Sudbury Neutrino Observatory". In: *Phys. Rev. Lett.* 89 (2002), p. 011301. DOI: 10.1103/PhysRevLett.89.011301. arXiv: nucl-ex/0204008.

[20] Jørgen Christensen-Dalsgaard. "Solar structure and evolution". In: *Living Reviews in Solar Physics* (2021). DOI: 10.1007/s41116-020-00028-3.

[21] J N Bahcall. "Solar Models and Solar Neutrinos". In: *Physica Scripta* T121 (Jan. 2005), pp. 46–50. ISSN: 1402-4896. DOI: 10.1088/0031-8949/2005/t121/006. URL: http://dx.doi.org/10.1088/0031-8949/2005/T121/006.

[22] S. Bilenky. "Neutrino oscillations: From a historical perspective to the present status". In: *Nuclear Physics B* 908 (2016). Neutrino Oscillations: Celebrating the Nobel Prize in Physics 2015, pp. 2–13. ISSN: 0550-3213. DOI: https://doi.org/10.1016/j.nuclphysb.2016.01.025. URL: https://www.sciencedirect.com/science/article/pii/S0550321316000353.

[23] B. Pontecorvo. "Mesonium and anti-mesonium". In: *Sov. Phys. JETP* 6 (1957), p. 429.

[24] B. Pontecorvo. "Neutrino Experiments and the Problem of Conservation of Leptonic Charge". In: *Zh. Eksp. Teor. Fiz.* 53 (1967), pp. 1717–1725.

[25] M. Acciarri et al. "Determination of the number of light neutrino species from single photon production at LEP". In: *Physics Letters B* 431.1 (1998), pp. 199–208. ISSN: 0370-2693. DOI: https://doi.org/10.1016/S0370-2693(98)00519-X. URL: https://www.sciencedirect.com/science/article/pii/S037026939800519X.

[26] Tsung-Han Yeh et al. "Probing physics beyond the standard model: limits from BBN and the CMB independently and combined". In: *Journal of Cosmology and Astroparticle Physics* 2022.10 (Oct. 2022), p. 046. ISSN: 1475-7516. DOI: 10.1088/1475-7516/2022/10/046. URL: http://dx.doi.org/10.1088/1475-7516/2022/10/046.

[27] Iván Esteban et al. "The fate of hints: updated global analysis of three-flavor neutrino oscillations". In: *JHEP* 09 (2020), p. 178. DOI: 10.1007/JHEP09(2020)178. arXiv: 2007.14792 [hep-ph].

[28] Iván Esteban et al. http://www.nu-fit.org/. NuFit 5.2. 2022.

[29] N. Aghanim et al. "Planck2018 results: VI. Cosmological parameters". In: *Astronomy amp; Astrophysics* 641 (Sept. 2020), A6. ISSN: 1432-0746. DOI: 10.1051/0004-6361/201833910. URL: http://dx.doi.org/10.1051/0004-6361/201833910.

[30] M. Aker et al. "Direct neutrino-mass measurement with sub-electronvolt sensitivity". In: *Nature Phys.* 18.2 (2022), pp. 160–166. DOI: 10.1038/s41567-021-01463-1. arXiv: 2105.08533 [hep-ex].

[31] L. Wolfenstein. "Neutrino oscillations in matter". In: *Phys. Rev. D* 17 (9 May 1978), pp. 2369–2374. DOI: 10.1103/PhysRevD.17.2369. URL: https://link.aps.org/doi/10.1103/PhysRevD.17.2369.

[32] S. P. Mikheyev and A. Yu. Smirnov. "Resonance enhancement of oscillations in matter and solar neutrino spectroscopy". In: *Yadernaya Fizika* 42 (Jan. 1985), pp. 1441–1448.

[33] C. A. Argüelles et al. "Snowmass white paper: beyond the standard model effects on neutrino flavor: Submitted to the proceedings of the US community study on the future of particle physics (Snowmass 2021)". In: *The European Physical Journal C* 83.1 (Jan. 2023). ISSN: 1434-6052. DOI: 10.1140/epjc/s10052-022-11049-7. URL: http://dx.doi.org/10.1140/epjc/s10052-022-11049-7.

[34] Victor Hess. *On the Observations of the Penetrating Radiation during Seven Balloon Flights*. 2018. arXiv: 1808.02927 [physics.hist-ph].

[35] Carmelo Evoli. *The Cosmic-Ray Energy Spectrum*. May 2023. DOI: 10.5281/zenodo.7948212. URL: https://doi.org/10.5281/zenodo.7948212.

[36] Carmelo Evoli. https://github.com/carmeloevoli/The_CR_Spectrum.

[37] Luis A. Anchordoqui. "Ultra-High-Energy Cosmic Rays". In: *Phys. Rept.* 801 (2019), p. 1. DOI: 10.1016/j.physrep.2019.01.002. arXiv: 1807.09645 [astro-ph.HE].

[38] Rafael Alves Batista et al. "Open Questions in Cosmic-Ray Research at Ultra-high Energies". In: *Front. Astron. Space Sci.* 6 (2019), p. 23. DOI: 10.3389/fspas.2019.00023. arXiv: 1903.06714 [astro-ph.HE].

[39] Charles Dermer and Govind Menon. *High Energy Radiation From Black Holes: Gamma Rays, Cosmic Rays, and Neutrinos*. Princeton University Press, 2009.

[40] Malcolm S. Longair. *High Energy Astrophysics*. 3rd ed. Cambridge University Press, 2011.

[41] A. De Angelis, G. Galanti, and M. Roncadelli. "Transparency of the Universe to gamma-rays". In: *Monthly Notices of the Royal Astronomical Society* 432.4 (May 2013), pp. 3245–3249. ISSN: 0035-8711. DOI: 10.1093/mnras/stt684. eprint: https://academic.oup.com/mnras/article-pdf/432/4/3245/18603541/stt684.pdf. URL: https://doi.org/10.1093/mnras/stt684.

[42] Eli Waxman and John N. Bahcall. "High-energy neutrinos from astrophysical sources: An Upper bound". In: *Phys. Rev. D* 59 (1999), p. 023002. DOI: 10.1103/PhysRevD.59.023002. arXiv: hep-ph/9807282.

[43] Christian Spiering. "Towards high-energy neutrino astronomy: A historical review". In: *The European Physical Journal H* 37.3 (July 2012), pp. 515–565. ISSN: 2102-6467. DOI: 10.1140/epjh/e2012-30014-2. URL: http://dx.doi.org/10.1140/epjh/e2012-30014-2.

[44] M.G. Aartsen et al. "The IceCube Neutrino Observatory: instrumentation and online systems". In: *Journal of Instrumentation* 12.03 (Mar. 2017), P03012–P03012. ISSN: 1748-0221. DOI: 10.1088/1748-0221/12/03/p03012. URL: http://dx.doi.org/10.1088/1748-0221/12/03/P03012.

[45] M. G. Aartsen et al. "Detection of a particle shower at the Glashow resonance with IceCube". In: *Nature* 591.7849 (Mar. 2021), pp. 220–224. ISSN: 1476-4687. DOI: 10.1038/s41586-021-03256-1. URL: http://dx.doi.org/10.1038/s41586-021-03256-1.

[46] IceCube Collaboration. https://icecube.wisc.edu/science/icecube/.

[47] John G. Learned and Sandip Pakvasa. "Detecting tau-neutrino oscillations at PeV energies". In: *Astropart. Phys.* 3 (1995), pp. 267–274. DOI: 10.1016/0927-6505(94)00043-3. arXiv: hep-ph/9405296.

[48] IceCube Collaboration. *Observation of Seven Astrophysical Tau Neutrino Candidates with IceCube*. 2024. arXiv: 2403.02516 [astro-ph.HE].

[49] R. Abbasi et al. "Detection of astrophysical tau neutrino candidates in IceCube". In: *Eur. Phys. J. C* 82.11 (2022), p. 1031. DOI: 10.1140/epjc/s10052-022-10795-y. arXiv: 2011.03561 [hep-ex].

[50] Mark G. Aartsen et al. "First observation of PeV-energy neutrinos with IceCube". In: *Phys. Rev. Lett.* 111 (2013), p. 021103. DOI: 10.1103/PhysRevLett.111.021103. arXiv: 1304.5356 [astro-ph.HE].

[51] Mark G. Aartsen et al. "Evidence for High-Energy Extraterrestrial Neutrinos at the IceCube Detector". In: *Science* 342 (2013), p. 1242856. DOI: 10.1126/science.1242856. arXiv: 1311.5238 [astro-ph.HE].

[52] Mark G. Aartsen et al. "Observation of High-Energy Astrophysical Neutrinos in Three Years of IceCube Data". In: *Phys. Rev. Lett.* 113 (2014), p. 101101. DOI: 10.1103/PhysRevLett.113.101101. arXiv: 1405.5303 [astro-ph.HE].

[53] Rasha U. Abbasi et al. "The IceCube high-energy starting event sample: Description and flux characterization with 7.5 years of data". In: *Phys. Rev. D* 104 (2021), p. 022002. DOI: 10.1103/PhysRevD.104.022002. arXiv: 2011.03545 [astro-ph.HE].

[54] Mark G. Aartsen et al. "Observation and Characterization of a Cosmic Muon Neutrino Flux from the Northern Hemisphere using six years of IceCube data". In: *Astrophys. J.* 833.1 (2016), p. 3. DOI: 10.3847/0004-637X/833/1/3. arXiv: 1607.08006 [astro-ph.HE].

[55] R. Abbasi et al. "Evidence for neutrino emission from the nearby active galaxy NGC 1068". In: *Science* 378.6619 (2022), pp. 538–543. DOI: 10.1126/science.abg3395. arXiv: 2211.09972 [astro-ph.HE].

[56] M. G. Aartsen et al. "Characteristics of the diffuse astrophysical electron and tau neutrino flux with six years of IceCube high energy cascade data". In: *Phys. Rev. Lett.* 125.12 (2020), p. 121104. DOI: 10.1103/PhysRevLett.125.121104. arXiv: 2001.09520 [astro-ph.HE].

[57] M. G. Aartsen et al. "Neutrino emission from the direction of the blazar TXS 0506+056 prior to the IceCube-170922A alert". In: *Science* 361.6398 (2018), pp. 147–151. DOI: 10.1126/science.aat2890. arXiv: 1807.08794 [astro-ph.HE].

[58] Davide Miceli and Lara Nava. "Gamma-Ray Bursts Afterglow Physics and the VHE Domain". In: *Galaxies* 10.3 (May 2022), p. 66. ISSN: 2075-4434. DOI: 10.3390/galaxies10030066. URL: http://dx.doi.org/10.3390/galaxies10030066.

[59] P. Padovani et al. "Active galactic nuclei: what's in a name?" In: *The Astronomy and Astrophysics Review* 25.1 (Aug. 2017). ISSN: 1432-0754. DOI: 10.1007/s00159-017-0102-9. URL: http://dx.doi.org/10.1007/s00159-017-0102-9.

[60] Suvi Gezari. "Tidal Disruption Events". In: *Ann. Rev. Astron. Astrophys.* 59 (2021), pp. 21–58. DOI: 10.1146/annurev-astro-111720-030029. arXiv: 2104.14580 [astro-ph.HE].

[61] M. G. Aartsen et al. "The IceCube Realtime Alert System". In: *Astropart. Phys.* 92 (2017), pp. 30–41. DOI: 10.1016/j.astropartphys.2017.05.002. arXiv: 1612.06028 [astro-ph.HE].

[62] R. Abbasi et al. "Observation of high-energy neutrinos from the Galactic plane". In: *Science* 380.6652 (2023), adc9818. DOI: 10.1126/science.adc9818. arXiv: 2307.04427 [astro-ph.HE].

[63] Veniamin S. Berezinsky and George T. Zatsepin. "Cosmic rays at ultrahigh-energies (neutrino?)" In: *Phys. Lett. B* 28 (1969), p. 423. DOI: 10.1016/0370-2693(69)90341-4.

[64] Victor Branco Valera, Mauricio Bustamante, and Christian Glaser. "Near-future discovery of the diffuse flux of ultrahigh-energy cosmic neutrinos". In: *Phys. Rev. D* 107.4 (2023), p. 043019. DOI: 10.1103/PhysRevD.107.043019. arXiv: 2210.03756 [astro-ph.HE].

[65] Ke Fang et al. "Testing the Newborn Pulsar Origin of Ultrahigh Energy Cosmic Rays with EeV Neutrinos". In: *Phys. Rev. D* 90.10 (2014). [Erratum: Phys. Rev. D 92, 129901 (2015)], p. 103005. DOI: 10.1103/PhysRevD.90.103005. arXiv: 1311.2044 [astro-ph.HE].

[66] Paolo Padovani et al. "A simplified view of blazars: the neutrino background". In: *Mon. Not. Roy. Astron. Soc.* 452.2 (2015), p. 1877. DOI: 10.1093/mnras/stv1467. arXiv: 1506.09135 [astro-ph.HE].

[67] Ke Fang and Kohta Murase. "Linking High-Energy Cosmic Particles by Black Hole Jets Embedded in Large-Scale Structures". In: *Nature Phys.* 14.4 (2018), p. 396. DOI: 10.1038/s41567-017-0025-4. arXiv: 1704.00015 [astro-ph.HE].

[68] Jonas Heinze et al. "A new view on Auger data and cosmogenic neutrinos in light of different nuclear disintegration and air-shower models". In: *Astrophys. J.* 873.1 (2019), p. 88. DOI: 10.3847/1538-4357/ab05ce. arXiv: 1901.03338 [astro-ph.HE].

[69] Marco Stein Muzio, Michael Unger, and Glennys R. Farrar. "Progress towards characterizing ultrahigh energy cosmic ray sources". In: *Phys. Rev. D* 100.10 (2019), p. 103008. DOI: 10.1103/PhysRevD.100.103008. arXiv: 1906.06233 [astro-ph.HE].

[70] Xavier Rodrigues et al. "Active Galactic Nuclei Jets as the Origin of Ultrahigh-Energy Cosmic Rays and Perspectives for the Detection of Astrophysical Source Neutrinos at EeV Energies". In: *Phys. Rev. Lett.* 126.19 (2021), p. 191101. DOI: 10.1103/PhysRevLett.126.191101. arXiv: 2003.08392 [astro-ph.HE].

[71] Astrid Anker et al. "White Paper: ARIANNA-200 high energy neutrino telescope". In: (Apr. 2020). arXiv: 2004.09841 [astro-ph.IM].

[72] Marco Stein Muzio, Glennys R. Farrar, and Michael Unger. "Probing the environments surrounding ultrahigh energy cosmic ray accelerators and their implications for astrophysical neutrinos". In: *Phys. Rev. D* 105.2 (2022), p. 023022. DOI: 10.1103/PhysRevD.105.023022. arXiv: 2108.05512 [astro-ph.HE].

[73] Rasha U. Abbasi et al. "Improved Characterization of the Astrophysical Muon–neutrino Flux with 9.5 Years of IceCube Data". In: *Astrophys. J.* 928.1 (2022), p. 50. DOI: 10.3847/1538-4357/ac4d29. arXiv: 2111.10299 [astro-ph.HE].

[74] M. G. Aartsen et al. "Differential limit on the extremely-high-energy cosmic neutrino flux in the presence of astrophysical background from nine years of IceCube data". In: *Physical Review D* 98.6 (Sept. 2018). ISSN: 2470-0029. DOI: 10.1103/physrevd.98.062003. URL: http://dx.doi.org/10.1103/PhysRevD.98.062003.

[75] Ek Paudel, Alan Coleman, and Frank Schröder. "Parametrization of the Relative Amplitude of Geomagnetic and Askaryan Radio Emission from Cosmic-Ray Air Showers using CORSIKA/CoREAS Simulations". In: July 2021, p. 429. DOI: 10.22323/1.395.0429.

[76] Juan A. Aguilar et al. "Design and Sensitivity of the Radio Neutrino Observatory in Greenland (RNO-G)". In: *JINST* 16.03 (2021), P03025. DOI: 10.1088/1748-0221/16/03/P03025. arXiv: 2010.12279 [astro-ph.IM].

[77] Yue Pan et al. "A neural network based UHE neutrino reconstruction method for the Askaryan Radio Array (ARA)". In: *PoS* ICRC2021 (2021), p. 1157. DOI: 10.22323/1.395.1157.

[78] Steven W. Barwick et al. "Capabilities of ARIANNA: Neutrino Pointing Resolution and Implications for Future Ultra-high Energy Neutrino Astronomy". In: *PoS* ICRC2021 (2021), p. 1151. DOI: 10.22323/1.395.1151.

[79] Peter W. Gorham et al. "Constraints on the ultrahigh-energy cosmic neutrino flux from the fourth flight of ANITA". In: *Phys. Rev. D* 99.12 (2019), p. 122001. DOI: 10.1103/PhysRevD.99.122001. arXiv: 1902.04005 [astro-ph.HE].

[80] Ilya Kravchenko et al. "Updated Results from the RICE Experiment and Future Prospects for Ultra-High Energy Neutrino Detection at the South Pole". In: *Phys. Rev. D* 85 (2012), p. 062004. DOI: 10.1103/PhysRevD.85.062004. arXiv: 1106.1164 [astro-ph.HE].

[81] Mark G. Aartsen et al. "IceCube-Gen2: the window to the extreme Universe". In: *J. Phys. G* 48.6 (2021), p. 060501. DOI: 10.1088/1361-6471/abbd48. arXiv: 2008.04323 [astro-ph.HE].

[82] Jaime Álvarez-Muñiz et al. "The Giant Radio Array for Neutrino Detection (GRAND): Science and Design". In: *Sci. China Phys. Mech. Astron.* 63.1 (2020), p. 219501. DOI: 10.1007/s11433-018-9385-7. arXiv: 1810.09994 [astro-ph.HE].

[83] Kumiko Kotera. "The Giant Radio Array for Neutrino Detection (GRAND) project". In: *PoS* ICRC2021 (2021), p. 1181. DOI: 10.22323/1.395.1181.

[84] P. Abreu et al. "Ultrahigh Energy Neutrinos at the Pierre Auger Observatory". In: *Advances in High Energy Physics* 2013 (2013), pp. 1–18. ISSN: 1687-7365. DOI: 10.1155/2013/708680. URL: http://dx.doi.org/10.1155/2013/708680.

[85] Federico Testagrossa, Damiano F. G. Fiorillo, and Mauricio Bustamante. *Two-detector flavor sensitivity to ultra-high-energy cosmic neutrinos*. 2023. arXiv: 2310.12215 [astro-ph.HE].

[86] F. W. Stecker and M. H. Salamon. "Photodisintegration of Ultra–High-Energy Cosmic Rays: A New Determination". In: *The Astrophysical Journal* 512.2 (Feb. 1999), pp. 521–526. ISSN: 1538-4357. DOI: 10.1086/306816. URL: http://dx.doi.org/10.1086/306816.

[87] Luis A Anchordoqui et al. "Galactic point sources of TeV antineutrinos". In: *Physics Letters B* 593.1–4 (July 2004), pp. 42–47. ISSN: 0370-2693. DOI: 10.1016/j.physletb.2004.04.054. URL: http://dx.doi.org/10.1016/j.physletb.2004.04.054.

[88] Roland M. Crocker et al. "The AGASA and SUGAR Anisotropies and TeV Gamma Rays from the Galactic Center: A Possible Signature of Extremely High Energy Neutrons". In: *The Astrophysical Journal* 622.2 (Apr. 2005), pp. 892–909. ISSN: 1538-4357. DOI: 10.1086/427972. URL: http://dx.doi.org/10.1086/427972.

[89] Rikard Enberg, Mary Hall Reno, and Ina Sarcevic. "High energy neutrinos from charm in astrophysical sources". In: *Phys. Rev. D* 79 (2009), p. 053006. DOI: 10.1103/PhysRevD.79.053006. arXiv: 0808.2807 [astro-ph].

[90] Jose Alonso Carpio et al. "Charm contribution to ultrahigh-energy neutrinos from newborn magnetars". In: *Phys. Rev. D* 102.10 (2020), p. 103001. DOI: 10.1103/PhysRevD.102.103001. arXiv: 2007.07945 [astro-ph.HE].

[91] Atri Bhattacharya et al. "Energy-dependent flavour ratios in neutrino telescopes from charm". In: (Sept. 2023). arXiv: 2309.09139 [astro-ph.HE].

[92] Ningqiang Song et al. "The Future of High-Energy Astrophysical Neutrino Flavor Measurements". In: *JCAP* 04 (2021), p. 054. DOI: 10.1088/1475-7516/2021/04/054. arXiv: 2012.12893 [hep-ph].

[93] M. G. Aartsen et al. "A combined maximum-likelihood analysis of the high-energy astrophysical neutrino flux measured with IceCube". In: *Astrophys. J.* 809.1 (2015), p. 98. DOI: 10.1088/0004-637X/809/1/98. arXiv: 1507.03991 [astro-ph.HE].

[94] M. G. Aartsen et al. "Measurements using the inelasticity distribution of multi-TeV neutrino interactions in IceCube". In: *Phys. Rev. D* 99.3 (2019), p. 032004. DOI: 10.1103/PhysRevD.99.032004. arXiv: 1808.07629 [hep-ex].

[95] Shi-Hao Wang et al. "Feasibility of Determining Diffuse Ultra-High Energy Cosmic Neutrino Flavor Ratio through ARA Neutrino Observatory". In: *JCAP* 11 (2013), p. 062. DOI: 10.1088/1475-7516/2013/11/062. arXiv: 1302.1586 [astro-ph.HE].

[96] Sigfrid Stjärnholm, Oscar Ericsson, and Christian Glaser. "Neutrino direction and flavor reconstruction from radio detector data using deep convolutional neural networks". In: *PoS* ICRC2021 (2021), p. 1055. DOI: 10.22323/1.395.1055.

[97] Christian Glaser, Daniel García-Fernández, and Anna Nelles. "Prospects for neutrino-flavor physics with in-ice radio detectors". In: *PoS* ICRC2021 (2021), p. 1231. DOI: 10.22323/1.395.1231.

[98] Alan Coleman et al. "The flavor composition of ultra-high-energy cosmic neutrinos: measurement forecasts for in-ice radio-based EeV neutrino telescopes". In: (Feb. 2024). arXiv: 2402.02432 [astro-ph.HE].

[99] Rasha U. Abbasi et al. "Sensitivity studies for the IceCube-Gen2 radio array". In: *PoS* ICRC2021 (2021), p. 1183. DOI: 10.22323/1.395.1183. arXiv: 2107.08910 [astro-ph.HE].

[100] Mark G. Aartsen et al. "Differential limit on the extremely-high-energy cosmic neutrino flux in the presence of astrophysical background from nine years of IceCube data". In: *Phys. Rev. D* 98.6 (2018), p. 062003. DOI: 10.1103/PhysRevD.98.062003. arXiv: 1807.01820 [astro-ph.HE].

[101] Alexander Aab et al. "Probing the origin of ultra-high-energy cosmic rays with neutrinos in the EeV energy range using the Pierre Auger Observatory". In: *JCAP* 10 (2019), p. 022. DOI: 10.1088/1475-7516/2019/10/022. arXiv: 1906.07422 [astro-ph.HE].

[102] Gary J. Feldman and Robert D. Cousins. "Unified approach to the classical statistical analysis of small signals". In: *Physical Review D* 57.7 (Apr. 1998), pp. 3873–3889. DOI: 10.1103/physrevd.57.3873. URL: https://doi.org/10.1103%2Fphysrevd.57.3873.

[103] Jakob van Santen et al. "toise: a framework to describe the performance of high-energy neutrino detectors". In: *JINST* 17.08 (2022), T08009. DOI: 10.1088/1748-0221/17/08/T08009. arXiv: 2202.11120 [astro-ph.IM].

[104] Christian Glaser et al. "NuRadioMC: Simulating the radio emission of neutrinos from interaction to detector". In: *Eur. Phys. J. C* 80.2 (2020), p. 77. DOI: 10.1140/epjc/s10052-020-7612-8. arXiv: 1906.01670 [astro-ph.IM].

[105] S. S. Wilks. "The Large-Sample Distribution of the Likelihood Ratio for Testing Composite Hypotheses". In: *Annals Math. Statist.* 9.1 (1938), pp. 60–62. DOI: 10.1214/aoms/1177732360.

[106] Mauricio Bustamante and Markus Ahlers. "Inferring the flavor of high-energy astrophysical neutrinos at their sources". In: *Phys. Rev. Lett.* 122.24 (2019), p. 241101. DOI: 10.1103/PhysRevLett.122.241101. arXiv: 1901.10087 [astro-ph.HE].

[107] Svenja Hümmer et al. "Simplified models for photohadronic interactions in cosmic accelerators". In: *Astrophys. J.* 721 (2010), p. 630. DOI: 10.1088/0004-637X/721/1/630. arXiv: 1002.1310 [astro-ph.HE].

[108] Walter Winter. "Photohadronic Origin of the TeV-PeV Neutrinos Observed in IceCube". In: *Phys. Rev. D* 88 (2013), p. 083007. DOI: 10.1103/PhysRevD.88.083007. arXiv: 1307.2793 [astro-ph.HE].

[109] Mauricio Bustamante and Irene Tamborra. "Using high-energy neutrinos as cosmic magnetometers". In: *Phys. Rev. D* 102.12 (2020), p. 123008. DOI: 10.1103/PhysRevD.102.123008. arXiv: 2009.01306 [astro-ph.HE].

[110] Poonam Mehta and Walter Winter. "Interplay of energy dependent astrophysical neutrino flavor ratios and new physics effects". In: *JCAP* 03 (2011), p. 041. DOI: 10.1088/1475-7516/2011/03/041. arXiv: 1101.2673 [hep-ph].

[111] Rasmus W. Rasmussen et al. "Astrophysical neutrinos flavored with Beyond the Standard Model physics". In: *Phys. Rev. D* 96.8 (2017), p. 083018. DOI: 10.1103/PhysRevD.96.083018. arXiv: 1707.07684 [hep-ph].

[112] Markus Ahlers, Klaus Helbing, and Carlos Pérez de los Heros. "Probing Particle Physics with IceCube". In: *Eur. Phys. J. C* 78.11 (2018), p. 924. DOI: 10.1140/epjc/s10052-018-6369-9. arXiv: 1806.05696 [astro-ph.HE].

[113] Markus Ackermann et al. "Fundamental Physics with High-Energy Cosmic Neutrinos". In: *Bull. Am. Astron. Soc.* 51 (2019), p. 215. arXiv: 1903.04333 [astro-ph.HE].

[114] Carlos A. Argüelles et al. "Fundamental physics with high-energy cosmic neutrinos today and in the future". In: *PoS* ICRC2019 (2020), p. 849. DOI: 10.22323/1.358.0849. arXiv: 1907.08690 [astro-ph.HE].

[115] Markus Ackermann et al. "High-energy and ultra-high-energy neutrinos: A Snowmass white paper". In: *JHEAp* 36 (2022), pp. 55–110. DOI: 10.1016/j.jheap.2022.08.001. arXiv: 2203.08096 [hep-ph].

[116] C. A. Argüelles et al. "Snowmass white paper: beyond the standard model effects on neutrino flavor: Submitted to the proceedings of the US community study on the future of particle physics (Snowmass 2021)". In: *Eur. Phys. J. C* 83.1 (2023), p. 15. DOI: 10.1140/epjc/s10052-022-11049-7. arXiv: 2203.10811 [hep-ph].

[117] Jorge Alfaro. "Quantum gravity and Lorentz invariance deformation in the standard model". In: *Phys. Rev. Lett.* 94 (2005), p. 221302. DOI: 10.1103/PhysRevLett.94.221302. arXiv: hep-th/0412295.

[118] Astrid Eichhorn, Alessia Platania, and Marc Schiffer. "Lorentz invariance violations in the interplay of quantum gravity with matter". In: *Phys. Rev. D* 102.2 (2020), p. 026007. DOI: 10.1103/PhysRevD.102.026007. arXiv: 1911.10066 [hep-th].

[119] Don Colladay and V. Alan Kostelecky. "Lorentz violating extension of the standard model". In: *Phys. Rev. D* 58 (1998), p. 116002. DOI: 10.1103/PhysRevD.58.116002. arXiv: hep-ph/9809521.

[120] V. Alan Kostelecky and Matthew Mewes. "Lorentz and CPT violation in neutrinos". In: *Phys. Rev. D* 69 (2004), p. 016005. DOI: 10.1103/PhysRevD.69.016005. arXiv: hep-ph/0309025.

[121] V. Alan Kostelecky and Neil Russell. "Data Tables for Lorentz and CPT Violation". In: *Rev. Mod. Phys.* 83 (2011), pp. 11–31. DOI: 10.1103/RevModPhys.83.11. arXiv: 0801.0287 [hep-ph].

[122] Jorge S. Díaz and Alan Kostelecky. "Lorentz- and CPT-violating models for neutrino oscillations". In: *Phys. Rev. D* 85 (2012), p. 016013. DOI: 10.1103/PhysRevD.85.016013. arXiv: 1108.1799 [hep-ph].

[123] R. Abbasi et al. "Search for quantum gravity using astrophysical neutrino flavour with IceCube". In: *Nature Phys.* 18.11 (2022), pp. 1287–1292. DOI: 10.1038/s41567-022-01762-1. arXiv: 2111.04654 [hep-ex].

[124] N. Aghanim et al. "Planck 2018 results. VI. Cosmological parameters". In: *Astron. Astrophys.* 641 (2020). [Erratum: Astron. Astrophys. 652, C4 (2021)], A6. DOI: 10.1051/0004-6361/201833910. arXiv: 1807.06209 [astro-ph.CO].

[125] Shaun Cole et al. "The 2dF Galaxy Redshift Survey: Near infrared galaxy luminosity functions". In: *Mon. Not. Roy. Astron. Soc.* 326 (2001), p. 255. DOI: 10.1046/j.1365-8711.2001.04591.x. arXiv: astro-ph/0012429.

[126] Andrew M. Hopkins and John F. Beacom. "On the normalisation of the cosmic star formation history". In: *Astrophys. J.* 651 (2006), p. 142. DOI: 10.1086/506610. arXiv: astro-ph/0601463.

[127] Glen Cowan et al. "Asymptotic formulae for likelihood-based tests of new physics". In: *Eur. Phys. J. C* 71 (2011). [Erratum: Eur. Phys. J. C 73, 2501 (2013)], p. 1554. DOI: 10.1140/epjc/s10052-011-1554-0. arXiv: 1007.1727 [physics.data-an].

[128] M. G. Aartsen et al. “Neutrino Interferometry for High-Precision Tests of Lorentz Symmetry with IceCube”. In: *Nature Phys.* 14.9 (2018), pp. 961–966. DOI: 10.1038/s41567-018-0172-2. arXiv: 1709.03434 [hep-ex].

[129] Angela V. Olinto et al. “The POEMMA (Probe of Extreme Multi-Messenger Astrophysics) observatory”. In: *JCAP* 06 (2021), p. 007. DOI: 10.1088/1475-7516/2021/06/007. arXiv: 2012.07945 [astro-ph.IM].